JCI insight

The histone methyltransferase SUV420H2 regulates brown and beige adipocyte thermogenesis

Xin Cui, … , Hang shi, Bingzhong Xue

JCI Insight. 2024. https://doi.org/10.1172/jci.insight.164771.

Research In-Press Preview Metabolism

Activation of brown adipose tissue (BAT) thermogenesis increases energy expenditure and alleviates obesity. Here we discover that histone methyltransferase suppressor of variegation 4-20 homolog 2 (Suv420h2) expression parallels that of Ucp1 in brown and beige adipocytes and that Suv420h2 knockdown significantly reduces, whereas Suv420h2 overexpression significantly increases Ucp1 levels in brown adipocytes. Suv420h2 knockout (H2KO) mice exhibit impaired cold-induced thermogenesis and are prone to diet-induced obesity. In contrast, mice with specific overexpression of Suv420h2 in adipocytes display enhanced cold-induced thermogenesis and are resistant to diet-induced obesity. Further study shows that Suv420h2 catalyzes H4K20 trimethylation at eukaryotic translation initiation factor 4E-binding protein 1 (4e-bp1) promoter, leading to down-regulated expression of 4e-bp1, a negative regulator of the translation initiation complex. This in turn up-regulates PGC1α protein levels, which is associated with increased expression of thermogenic program. We conclude that Suv420h2 is a key regulator of brown/beige adipocyte development and thermogenesis.

The Histone Methyltransferase SUV420H2 Regulates Brown and Beige Adipocyte Thermogenesis

Xin Cui[1], Qiang Cao[1], Fenfen Li[1], Jia Jing[1], Zhixue Liu[1], Xiaosong Yang[1,2], Gary J. Schwartz[3], Liqing Yu[4], Huidong Shi[5,6], Hang Shi[1*], Bingzhong Xue[1*]

[1]Department of Biology, Georgia State University, Atlanta, GA 30303, USA.

[2]Present address: Hubei Key Laboratory of Diabetes and Angiopathy, Hubei University of Science and Technology, Xianning, 437100, China

[3]Department of Medicine, Albert Einstein College of Medicine, Bronx, NY 10461

[4]Department of Medicine, University of Maryland School of Medicine, Baltimore, MD, USA.

[5]Georgia Cancer Center, and [6]Department of Biochemistry and Molecular Biology, Medical College of Georgia, Augusta University, Augusta, GA 30912, USA

* Correspondence should be addressed to:

Bingzhong Xue, Department of Biology, Georgia State University, Atlanta, GA 30303, USA. Contact: 404-413-5747, bxue@gsu.edu

Hang Shi, Department of Biology, Georgia State University, Atlanta, GA 30303, USA. Contact: 404-413-5799, hshi3@gsu.edu.

Abstract

Activation of brown adipose tissue (BAT) thermogenesis increases energy expenditure and alleviates obesity. Here we discover that histone methyltransferase suppressor of variegation 4-20 homolog 2 (*Suv420h2)* expression parallels that of *Ucp1* in brown and beige adipocytes and that *Suv420h2* knockdown significantly reduces, whereas *Suv420h2* overexpression significantly increases *Ucp1* levels in brown adipocytes. *Suv420h2* knockout (H2KO) mice exhibit impaired cold-induced thermogenesis and are prone to diet-induced obesity. In contrast, mice with specific overexpression of *Suv420h2* in adipocytes display enhanced cold-induced thermogenesis and are resistant to diet-induced obesity. Further study shows that *Suv420h2* catalyzes H4K20 trimethylation at eukaryotic translation initiation factor 4E-binding protein 1 (*4e-bp1*) promoter, leading to down-regulated expression of *4e-bp1*, a negative regulator of the translation initiation complex. This in turn up-regulates PGC1α protein levels, which is associated with increased expression of thermogenic program. We conclude that *Suv420h2* is a key regulator of brown/beige adipocyte development and thermogenesis.

Key words. SUV420H2, Histone methyltransferase, PGC1α, mitochondria, brown adipocytes, beige adipocytes, obesity.

Introduction

Obesity is a risk factor for a panel of metabolic disorders, including insulin resistance/type 2 diabetes, hypertension, fatty liver diseases, dyslipidemia, cardiovascular diseases and certain types of cancer. Persistent energy imbalance due to excess energy intake over energy expenditure results in obesity. The total energy expenditure can be divided into basic metabolic rate, physical activity and adaptive thermogenesis (1). Brown fat is a major player in adaptive thermogenesis (2, 3) due to the unique presence of UCP1 in mitochondrial inner membrane, which uncouples oxidative phosphorylation from ATP synthesis, thereby dissipating energy as heat (2, 3). Recent studies also point to several UCP1-independent mechanisms in thermogenesis (4, 5). Rodents have two types of brown adipocytes: classic brown adipose tissue (BAT) is mainly confined to interscapular area and newly discovered beige adipocytes or beige fat (BeAT) is sporadically dispersed in white adipose tissue (WAT) and can be induced by β-adrenergic activation (6-8).

Activation of brown/beige adipocyte thermogenesis increases energy expenditure and ameliorates obesity (9, 10). Given the recent discovery of thermogenic brown fat in humans (11-13), it is conceivable that brown/beige adipocyte thermogenesis is a promising target for therapeutic treatment of obesity.

Epigenetic mechanisms, including histone modifications have emerged as key links between environmental factors (e.g., diets) and complex diseases (e.g., obesity). However, how epigenetic mechanisms regulate brown/beige adipocyte function have been less explored. To identify functional epigenetic markers that regulate brown/beige adipocyte development, we surveyed the expression of most epigenetic enzymes, including histone methyltransferases, demethylases, and histone deacetylases, that catalyze histone methylation and acetylation during the early postnatal development of mouse beige adipocytes, and found that the expression pattern of suppressor of variegation 4-20 homolog 2 (Drosophila) (*Suv420h2*) mirrors that of *Ucp1*. Using genetic mouse models with loss- or gain- functions of *Suv420h2*, we determined the role of *Suv420h2* in cold-induced thermogenesis, energy metabolism and diet-induced obesity.

Results

Suv420h2 is important in regulating Ucp1 expression

Xue et al previously reported that beige adipocytes in WAT can be transiently induced in mice during early postnatal development, which peaked at 20 days of age and gradually disappeared thereafter (14). Although the mechanism underlying the transient induction of the developmental beige adipocytes remains

unclear, the expression pattern of *Ucp1* in WAT during this period offers a unique framework for identifying factors that regulate brown/beige cell development. Thus, we surveyed the expression patterns of most epigenetic enzymes, including histone methyltransferases, demethylases, and deacetylases, in mouse inguinal WAT (iWAT) during postnatal development from postnatal day 5 (P5) to day 120 (P120), and compared them to that of *Ucp1*. For the preliminary screening, we pooled 4 RNA samples from each time point. (14)We found that *Ucp1* expression in iWAT during postnatal development followed similar patterns to that observed in retroperitoneal WAT (rWAT) (14), peaked at P20 and gradually disappeared thereafter (**Supplemental Figure 1A**). Among the four genes encoding histone methyltransferases (*Suv420h1*, *Suv420h2*, and SET domain containing protein 8 (*Setd8*)), and demethylase PHD finger protein 8 (*Phf8*) that are responsible for histone H4 lysine 20 (H4K20) methylation, we discovered a unique expression pattern of *Suv420h2* (**Supplemental Figure 1B-E**), which mimicked that of *Ucp1*. We then further confirmed our results on *Ucp1* and *Suv420h2* expression using four individual RNA samples (**Figure 1A-B**). In adult rodents, *Suv420h2* expression was much higher in interscapular BAT (iBAT) than in other fat depots, including iWAT, epididymal WAT (eWAT) and rWAT (**Figure 1C**). We also found that *Suv420h2* expression was much higher than that of *Suv420h1* in adipose tissues (**Supplemental Figure 1F**). As expected, a 7-day cold exposure at 5°C in 2-3-month-old male mice stimulated *Ucp1* expression in iWAT (**Figure 1D**). Interestingly, *Suv420h2* expression parallels that of *Ucp1* in iWAT during cold exposure (**Figure 1E**).

In addition, differentiation of mouse immortalized brown adipocyte cell BAT1 (15, 16) is characterized by significant up-regulation of *Ucp1* expression (**Figure 1F**), which is paralleled by a gradual increase of *Suv420h2* expression (**Figure 1G**).

H4K20 can be mono-, di- and trimethylated (H4K20me1, H4K20me2 and H4K20me3, respectively) (17, 18). SETD8 is the only known monomethyltransferase; whereas SUV420H1 and SUV420H2 are responsible for di- and trimethylation of H4K20 (17, 18). We therefore further studied the roles of *Suv420h1*, *Suv420h2* and in gereral H4K20 methylation in regulating brown/beige adipocyte function. We found that knocking down *Suv420h2* with siRNA in BAT1 cells (**Supplemental Figure 2**) significantly decreased H4K20me3 levels around 50% without affecting H4K20me1 and H4K20me2 levels (**Figure 1H**); whereas overexpressing *Suv420h2* significantly increased H4K20me3 levels in BAT1 cells without changing H4K20me1 or H4K20me2 (**Figure 1I**).

Interestingly, knocking down *Suv420h2* in BAT1 cells significantly suppressed, whereas overexpressing *Suv420h2* significantly enhanced NE-stimulated *Ucp1* expression (**Figure 1J-K**).

Since knocking down *Suv420h2* resulted in around 50% reduction of H4K20me3 and both SUV420H1 and SUV420H2 catalyze H4K20 trimethylation, we also explored possible physiological function of *Suv420h1* in regulating brown adipocyte thermogenesis. Interestingly, overexpressing *Suv420h1* (**Supplemental Figure 3**) resulted in a significantly decreased NE-stimulated *Ucp1* expression (**Figure 1L**), indicating that *Suv420h1* and *Suv420h2* may have opposite effects on brown adipocyte thermogenic function. To further explore this possibility, we knocked down *Sub420h2* in BAT1 brown adipocytes and further treated cells with SUV420H1/H2 inhibitor A196 that has been shown to achieve an 80% reduction of H4K20me3 levels in treated cells (19). *Suv420h2* knockdown significantly reduced *Suv420h2* expression without changing *Suv420h1* levels in BAT1 cells; whereas combined *Suv420h2* knockdown and A196 treatment did not change *Suv420h1* expression nor did it further change *Suv420h2* expression (**Supplemental Figure 4A-B**). As expected, knocking down *Suv420h2* significantly suppressed NE-stimulated expression of genes important for brown adipocyte thermogenesis, including *ucp1* (**Figure 1M**), type 2 deiodinase (*Dio2*) (**Figure 1N**) and acyl-CoA thioesterase 2 (*Acot2*) (**Figure 1O**), a gene shown to facilitate mitochondrial fatty acid oxidation (20). Interestingly, combined treatment of BAT1 cells with *Suv420h2* knockdown and A196 reversed the inhibitory effects of *Suv420h2* knockdown on these gene expression levels, and restored them to that of control group (**Figure 1M-O**). These data collectively demonstrate that *Suv420h1* and *Suv420h2* regulates brown adipocyte thermogenesis, with *Suv420h2* serving as a potential positive regulator; whereas *suv420h1* may negatively regulate brown adipocyte thermogenesis.

<u>*Suv420h2 regulates the development of brown and beige fat*</u>

Recent data suggest that mice lacking both *Suv420h1* and *Suv420h2* exhibited increased mitochondria respiration in brown adipocytes, improved glucose tolerance, and were resistant to diet-induced obesity (21). However, since our *in vitro* data suggest that *Suv420h1* and *Suv420h2* may exert opposite effects on brown adipocyte function, it is important to delineate the functions of *Suv420h1* and *Suv420h2* separately in mouse models. Our gene expression data suggest that *Suv420h2* mirrors *Ucp1* expression during the postnatal development of beige adipocytes, we thus interrogated the role of *Suv420h2* in the development of brown and

beige adipocytes *in vivo*. We first examined brown and beige adipose tissue development in mice with whole body *Suv420h2* knockout (H2KO) (22) at postnatal day 20 (P20), when the developmental beige adipocytes appear at peak while brown fat development also ascends to mature (14). As expected, *Suv420h2* mRNA was not detectable in fat depots in H2KO mice, including iBAT, iWAT, eWAT and rWAT; in addition, there was also no difference in adipose tissue *Suv420h1* expression between WT and H2KO mice (**Supplemental Figure 5A-B**). Interestingly, iBAT from H2KO mice had significantly decreased UCP1 protein expression and less UCP1 staining compared to that of WT controls (**Figure 2A-B, Supplemental Figure 6A).** This was associated with enlarged adipocyte size (**Figure 2C**), as shown by a shift of significantly decreased smaller adipocyte and reciprocally increased larger adipocyte numbers in iBAT of 20-day-old H2KO mice compared to that of WT mice (**Figure 2D**). Likewise, iWAT from 20-day-old H2KO mice also had significantly lower UCP1 protein expression (**Figure 2E**) and less multilocular beige adipocytes with UCP1 staining (**Figure 2F, Supplemental Figure 6B-C**), suggesting a less appearance of the developmental beige adipocytes in iWAT of H2KO mice. In consistence, iWAT from 20-day-old H2KO mice had enlarged adipocyte size (**Figure 2G**), with a shift of significantly decreased smaller adipocyte and a tendency of reciprocally increased larger adipocyte numbers (**Figure 2H**).

We also generated transgenic mice (AH2Tg mice) overexpressing *Suv420h2* specifically in adipocytes under the control of adiponectin promoter (**Supplemental Figure 7A**). AH2Tg mice exhibited a significant increase of *Suv420h2* mRNA in all fat depots including iBAT, iWAT, eWAT and rWAT without affecting *Suv420h1* levels (**Supplemental Figure 7B-C**). iBAT from 20-day-old AH2Tg mice exhibited enhanced UCP1 protein levels and more UCP1 staining (**Figure 2I-J, Supplemental Figure 8A**). In addition, overexpression of *Suv420h2* in adipocytes resulted in reduced adipocyte size in iBAT during postnatal development at P20 (**Figure 2K**), as shown by a shift of significantly increased smaller adipocyte and a reciprocally decreased larger adipocyte number (**Figure 2L**). In consistence, AH2Tg mice exhibited higher UCP1 protein levels and more UCP1-positive multilocular beige adipocytes in iWAT (**Figure 2M-N, Supplemental Figure 8B-C**). iWAT from AH2Tg mice also exibited reduced adipocyte size (**Figure 2O**), as shown by a shift of significantly increased smaller adipocyte and reciprocally decreased larger adipocyte number (**Figure 2P**). In sum, these data suggest that *Suv420h2* promotes brown and beige adipocytes formation during the postnatal development.

Suv420h2 regulates cold-induced thermogenesis

In adult mice, beige adipocytes can be induced by chronic cold exposure. To determine the role of *Suv420h2* in cold-induced brown and beige adipocyte thermogenesis, we subjected 3-month-old male H2KO, AH2Tg and their respective WT littermates to a chronic 7-day cold challenge. During the cold exposure, H2KO mice displayed significantly lower body temperature compared to their littermate controls (**Figure 3A**), suggesting that *Suv420h2* deficiency causes cold intolerance. Moreover, H2KO mice had higher fat mass in iWAT, eWAT and rWAT after the cold challenge (**Figure 3B**), suggesting a less efficiency in utilizing stored energy in fat depots. This was consistent with larger adipocytes observed in both iBAT and iWAT of H2KO mice (**Figure 3C**), witha shift of reduced smaller adipocyte and a reciprocally increased larger adipocyte numbers in both iBAT and iWAT of cold-challenged H2KO mice, although the increase of larger adipocyte numbers in iWAT did not reach statistical significance (**Figure 3D**). In addition, cold-challenged H2KO mice exhibited decreased expression of *Ucp1* in both iBAT and iWAT (**Figure 3E-F**), along withreduced expression of other cold-induced thermogenic genes, including peroxisome proliferator activated receptor γ (*Pparγ*), cell death-inducing DNA fragmentation factor, alpha subunit-like effector A (*Cidea)*, muscle type carnitine palmitoyltransferase 1b (*Cpt1b*), epithelial V-like antigen 1 (*Eva1*), palmitoyl acyl-Coenzyme A oxidase 1 (*Acox1*) and cytochrome c oxidase subunit I (*Cox1*) in iBAT, and *Pparα*, PR domain containing 16 (*Prdm16*), *Cidea* and *Cpt1b* in iWAT (**Figure 3E-F**). As expected, *Suv420h2* deficiency resulted in decreased H4K20me3 levels in both iBAT and iWAT, along with decreased UCP1 protein levels (**Figure 3G-H**). Consistent with these findings, IHC analysis revealed less UCP1 staining in iBAT and less UCP1-positive beige adipocytes in iWAT of cold-challenged H2KO mice (**Figure 3I, Supplemental Figure 9A-C**). Seahorse analysis of primarily isolated brown adipocytes revealed reduced basal and maximal oxygen consumption rate (OCR) in H2KO mice relative to WT controls (**Figure 3J**), suggesting that *Suv420h2* deletion compromised mitochondrial function via a cell-autonomous manner.

In contrast, AH2Tg mice with adipocyte *Suv420h2* overexpression exhibited an opposite phenotype. Specifically, AH2Tg mice displayed higher body temperature compared to their littermate controls during the cold challenge (**Figure 4A**), suggesting an increased cold tolerance. Cold-challenged AH2Tg mice also had decreased fat mass in iWAT, eWAT and rWAT (**Figure 4B**). In consistence, iBAT and iWAT from cold-challenged AH2Tg mice had smaller adipocytes (**Figure 4C**), as shown by a shift of significantly increased smaller adipocyte and a tendency of reciprocally decreased larger adipocyte numbers (**Figure 4D**). In addition, iBAT and iWAT from cold-challenged AH2Tg mice exhibited enhanced expression of *Ucp1* and other thermogenic genes, such

as *Pparα*, Pparγ, *Cox1*, Otopetrin 1 (*Otop1*), *Eva1* and elongation of very long chain fatty acids (FEN1/Elo2, SUR4/Elo3, yeast)-like 3 (*Elovl3*) in iBAT, and *Pparα*, *Cidea, Cpt1b, Otop1 and Elovl3* in iWAT (**Figure 4E-F**). Moreover, *Suv420h2* overexpression in adipocytes led to a significant increase in H4K20me3 as well as UCP1 levels in both iBAT and iWAT, (**Figure 4G-H**). In consistent with these findings, IHC analysis revealed a stronger UCP1 staining in iBAT and higher UCP1-positive beige adipocyte induction in iWAT (**Figure 4I, Supplemental Figure 10A-C**). In addition, Seahorse analysis revealed enhanced maximal oxygen consumption rate (OCR) in primary adipocytes isolated from AH2Tg mice (**Figure 4J**), suggesting that *Suv420h2* overexpression increases mitochondrial function in a cell-autonomous manner.

Suv420h2 regulates mitochondrial bioenergetic program

To gain further insight into how *Suv420h2* regulates brown/beige fat thermogenesis, we performed RNAseq analysis in iWAT of 7-day-cold-challenged H2KO and AH2Tg mice. Analysis of differentially expressed genes with online software (https://github.com/PerocchiLab/ProFAT) (23) predicted an overall reduced browning probability in *Suv420h2*-deficient iWAT, with a reciprocal increase in gene expression profile resembling that of WAT (**Figure 5A**). This was consistent with a down-regulation of BAT-specific, and an up-regulation of WAT-specific gene expression in *Suv420h2*-deficient iWAT (**Figure 5A)**. In contrast, analysis of differentially expressed genes in iWAT between WT and AH2Tg mice revealed an overall enhanced browning probability, evidenced by enhanced BAT-specific, and reduced WAT-specific gene expression (**Figure 5B**). Interestingly, we found that groups of BAT-specific genes were reciprocally regulated in iWAT between H2KO and AH2Tg mice, including *Ucp1*, *Ucp3*, *Cpt1b*, *Otop1*, *Kcnk3*, *S100b* (**Figure 5A-C**), highlighting the importance of *Suv420h2* in beige fat thermogenesis. More strikingly, genes involved in mitochondrial bioenergetic pathways, including electron transport chain, fatty acid β-oxidation and TCA cycle stood out as converged pathways that were down- or up-regulated in H2KO and AH2Tg mice, respectively (**Figure 5D** and **Supplemental Figure 11A-B**).

To further investigate how SUV420H2 regulates pathways in mitochondria function and thermogenesis, we performed assay for transposase-accessible chromatin sequencing (ATAC-seq) analysis in iBAT of 7-day-cold-challenged WT and AH2Tg mice. We compared genome-wide alterations in chromatin accessibility landscape assessed by ATAC-seq with that of gene expression patterns assessed by RNA-seq and discovered a strong correlation between chromatin accessibility status and gene expression changes. As illustrated in **Figure 5E**,

the decreases in read densities of genes of two selective clusters (Clusters 1 and 2, **Figure 5E**) based on variable degree of peaks in AH2Tg iBAT, which indicates less chromatin accessibility, were highly associated with the down-regulations of the corresponding gene expression, including several genes known to negatively regulate brown/beige adipocyte thermogenesis and energy metabolism, such as nicotinamide N-methyltransferase (*Nnmt*)(24), natriuretic peptide receptor 3 (*Npr3*)(25), twist basic helix-loop-helix transcription factor 1 (*Twist1*)(26) and zinc finger protein 423 (*Zfp423*)(27). In addition, we also identified two clusters of genes that showed more chromatin accessibility and were associated with increased gene expression (Clusters 3 and 4, **Figure 5E**), including several genes encoding mitochondrial electron transporting chain proteins, such as complex I component *Ndufa10*, complex III component ubiquinol-cytochrome c reductase, Rieske iron-sulfur polypeptide 1 (*Uqcrfs1*) and complex IV component heme A:farnesyltransferase cytochrome c oxidase assembly factor 10 (*Cox10*).

Our data suggest that Suv420h2 regulates pathways involved in mitochondrial bioenergetics. Indeed, immunoblotting analysis of mitochondrial respiratory chain proteins revealed down regulation of complex I NADH dehydrogenase 1β subcomplex 8 (CI-NDUFB8), complex II succinate dehydrogenase complex, subunit B (CII-SDHB) and complex III cytochrome b-c1 complex subunit 2 (CIII-UQCRC2) in both iBAT and iWAT of H2KO mice (**Figure 6A-B**), while up-regulation of CI-NDUFB8, CII-SDHB and complex IV mitochondrially encoded cytochrome c oxidase I (CIV-MTCO1) in iBAT and iWAT of AH2Tg mice cold exposure (**Figure 6C-D**).

H4K20me3 is elevated at the promoter of 4E-BP1

Since genes responsible for mitochondrial function appears to be the most significant feature of *Suv420h2* regulated pathways, we next explored whether *Pgc1α*, the master regulator of mitochondrial biogenesis (28), is involved in this process. We first studied whether *Pgc1α* mRNA and protein levels were regulated during postnatal development and cold exposure. While both *Pgc1α* mRNA and protein levels were significantly higher in iWAT of 20-day-old mice compared to that of 3-month-old mice (**Figure 7A-B**), H4K20me3 level at *Pgc1α* promoter was not significantly different in iWAT across the developmental course (**Supplemental Figure 12**). Further, while *Pgc1α* mRNA expression was only transiently up-regulated in iWAT one day after cold exposure, cold-induced increase in PGC1α protein levels was observed at seven days after cold exposure (**Figure 7C-D**). These data suggest that *Pgc1α* expression may not depend on promoter H4K20 trimethylation,

and PGC1α protein level may be regulated independent of mRNA expression, at least during chronic cold exposure.

Similarly, although our ATACseq and RNAseq data suggested that overexpressing *Suv420h2* in adipocytes resulted in a more open chromatin structure at *Pgc1α* locus, along with increased *Pgc1α* expression peaks (**Supplemental Figure 13A**), quantitative RT-PCR analysis showed that *Pgc1α* expression was not significantly changed in iBAT and iWAT of H2KO (**Figure 3E-F**) or AH2Tg mice (**Figure 4E-F**) after cold exposure. We also did not observe any changes in *Pgc1α* expression in BAT1 brown adipocytes with *Suv420h2* knockdown and with combined *Suv420h2* knockdown and A196 treatment (**Supplemental Figure 13B**). Interestingly, *Suv420h2* deletion in H2KO mice decreased, while Suv420h2 overexpressing in AH2Tg mice increased PGC1α protein content in both iBAT and iWAT (**Figure 7E-F, 7G-H**). Thus, our data suggest that PGC1α protein level may be regulated independently of its mRNA expression, and Suv420h2 may be involved in the regulation of PGC1α protein levels.

PGC1α is a short-lived protein and therefore its protein level is tightly regulated by either protein synthesis or degradation. PGC1α protein levels can be regulated by protein degradation (29, 30) or synthesis (31). The E3 ligases F-box and WD-40 domain protein 7 (FBXW7) and ring finger protein 34 (RNF34) have been previously shown to promote PGC1α protein ubiquitination and degradation (29, 30), whereas PGC1α protein translation can be regulated by the eukaryotic translation initiation eIF4F complex, as the negative regulator of the eIF4F complex, the eukaryotic translation initiation factor 4E binding protein 1 (4E-BP1), has been shown to negatively regulate PGC1α protein synthesis (31). There was no change in the expression of *Fbxw7* and *Rnf34* between WT and H2KO, and between WT and H2Tg mice (**Supplemental Figure 14**). (31)Interestingly, our ATACseq and RNAseq data suggest that overexpressing *Suv420h2* in adipocytes resulted in a more closed chromatin structure at *4e-bp1* locus, which was associated with reduced *4e-bp1* expression (**Figure 8A**). Indeed, *4e-bp1* expression was significantly up-regulated in iBAT and iWAT of cold-challenged H2KO mice, but tended to decrease in iBAT and was significantly decreased in iWAT and eWAT of cold-challenged AH2Tg mice (**Figure 8B-C**). In consistence, 4E-BP1 protein levels in iBAT and iWAT were increased in cold-challenged H2KO mice, but decreased in cold-challenged AH2Tg mice (**Figure 8D-E, 8F-G**).

We also measured 4E-BP1 protein levels in iWAT of C57BL/6J mice during postnatal development and cold challenge. Interestingly, 4E-BP1 protein levels were significantly increased in iWAT of 3-month-old mice as

compared to that of 20-day-old mice (**Figure 8H**). Since 4E-BP1 negatively regulates PGC1α protein levels (31), this may explain the decreased PGC1α protein levels in iWAT of 3-month-old mice (**Figure 7-B**). On the other hand, cold exposure significantly reduced 4E-BP1 protein levels (**Figure 8H**), which may contribute to the increased PGC1α protein levels in iWAT of cold-challenged mice (**Figure 7-D**).

Mechanistically, ChIP assay revealed that H4K20me3 levels at *4e-bp1* promoter (**Supplemental Figure 15**) (32-34) was significantly decreased in both iBAT and iWAT of H2KO mice (**Figure 9A-B**).Thus, *Suv420h2* deletion may decrease histone repressive mark H4K20me3 at *4e-bp1* locus, resulting in increased *4e-bp1* expression, which could lead to decreased PGC1α protein levels seen in H2KO mice. In contrast, *Suv420h2* overexpression in AH2Tg mice increased *4e-bp1* promoter H4K20me3 levels in iBAT and iWAT (**Figure 9C-D**), which may lead to decreased expression of *4e-bp1,* potentially contributing to increased PGC1α protein levels observed in AH2Tg mice.

To further confirm that SUV420H2 regulates PGC1α protein levels via regulation of *4e-bp1* expression, we knocked down both *Suv420h2* and *4e-bp1* in BAT1 brown adipocytes. As shown in **Figure 9E**, knocking down *Suv420h2* significantly increased 4E-BP1 levels in BAT1 brown adipocytes, similarly to those observed in H2KO mice (**Figure 8D-E**); whereas combined knockdown of both *Suv420h2* and *4e-bp1* significantly reduced 4E-BP1 levels (**Figure 9E**). Interestingly, knocking down of *Suv420h2* tended to reduce basal PGC1α protein levels, and significantly reduced NE-stimulated PGC1α protein levels in BAT1 brown adipocytes. Further knocking down of *4e-bp1* blocked this effect, and restored PGC1α protein level to that of control group (**Figure 9F**). These data suggest that 4E-BP1 mediates SUV420H2's effect on regulating PGC1α protein levels.

We also explored other possible SUV420H2 downstream targets that could potentially mediate SUV420H2's function in regulating brown/beige adipocyte function. Pedrotti et al (21) reported that deletion of both *Suv420h1* and *Suv420h2* resulted in enhanced mitochondria respiration in brown adipocytes, possibly via up-regulation of the expression of *Pparγ*, a master regulator of brown and white adipocyte lipid and glucose metabolism, and thermogenic function (35, 36). However, we observed no difference in chromatin accessibility and RNA expression peaks at *Pparγ* locus in our ATACseq and RNAseq data from cold-challenged WT and AH2Tg mice (**Supplemental Figure 16A**). In addition, there were no consistent changes in cold-induced *Pparγ* mRNA (**Figures 3E-F and 4E-F**) and protein (**Supplemental Figure 16B-C**) levels in iBAT and iWAT between WT and H2KO mice and between WT and AH2Tg mice.

Prdm16 is emerged as an important regulator of brown adipocyte development (16, 37). However, we did not observe any differences in chromatin accessibility and RNA expression at *Prdm16* locus in our ATACseq and RNAseq data (**Supplemental Figure 17A**). In addition, there were no consistent changes in cold-induced *Prdm16* mRNA (**Figure 3E-F, Figure 4E-F**) and protein (**Supplemental Figure 17B-C**) levels in iBAT and iWAT between WT and H2KO mice and between WT and AH2Tg mice.

Twist1 and *Zfp423* negatively regulate brown/beige adipocyte thermogenesis and energy homeostasis (26, 27). *Twist1* interacts with PGC1α on PGC1α-target genes to suppress mitochondrial metabolism and uncoupling (26); whereas *Zfp423* suppresses adipocyte thermogenic capacity by interfering with several important factors for brown adipocyte function, such as early B cell factor 2 (*Ebf2*) and *Prdm16* (27, 38). Our ATACseq and RNAseq data indicated that chromatin accessibility and RNA expression peaks at *Twist1* and *Zfp423* loci (**Supplemental Figure 18A and 19A**) were decreased in WT and AH2Tg mice after cold exposure. In addition, the expression of *Twist 1* (**Supplemental Figure 18B-C**) and *Zfp423* (**Supplemental Figure 19B-C**) was increased in iWAT of H2KO mice but reciprocally decreased in iWAT of AH2Tg mice after cold exposure. However, ChIP assay demonstrated that H4K20me3 levels at *Twist1* (**Supplemental Figure 18D-E**) or *Zfp423* (**Supplemental Figure 19D-E**) promoter was not different in iBAT and iWAT between cold-challenged WT and H2KO mice and between cold-challenged WT and AH2Tg mice. (Thus, while changes in *Twist1* and *Zfp423* expression might potentially contribute to altered brown/beige adipocyte function observed in our H2KO and AH2Tg mice, they are not likely mediated via *Suv420h2*-regulated H4K20 methylation.

Estrogen-related receptor gamma (*Esrrg*) is emerged as a positive regulator of mitochondrial oxidative metabolism and thermogenesis via both *Pgc1α*-dependent and independent mechanisms (39, 40). Our ATACseq and RNAseq data indicated that chromatin accessibility and RNA expression peaks at *Esrrg* locus were increased in cold-challenged WT and AH2Tg mice (**Supplemental Figure 20A**). In addition, *Esrrg* mRNA and protein levels were decreased in iWAT of H2KO mice (**Supplemental Figure 20B-C**) but reciprocally increased in iWAT of AH2Tg mice (**Supplemental Figure 20D-E**) after cold exposure. However, H4K20me3 level at *Esrrg* promoter was not different in iBAT and iWAT between H2KO and WT (**Supplemental Figure 20F-G**) and between AH2Tg and WT mice (**Supplemental Figure 20H-I**), suggesting the altered *Esrrg* expression in H2KO and AH2Tg mice was not dependent on *Suv420h2*.

We further investigated whether ESRRG protein level could be regulated by 4E-BP1. As shown in **Supplemental Figure 20J**, *Suv420h2* knockdown significantly reduced NE-stimulated ESRRG protein levels in BAT1 cells; however, further knockdown of *4e-bp1* blocked this effect and restored ESRRG protein levels to that of control group. Thus, *Esrrg* may be another potential target besides *Pgc1α* mediating *Suv420h2*'s effect on brown/beige adipocyte thermogenesis. However, similarly to that of *Pgc1α*, *Esrrg* may not be a direct target of *Suv420h2*, as *Esrrg* promoter H4K20me3 levels in iBAT and iWAT were not different in cold-challenged H2KO and AH2Tg mice compared to their respective WT controls. Instead, ESRRG protein levels may be regulated by 4E-BP1-mediated translational regulation, similarly to that of PGC1α.

We further explored whether other brown/beige adipocyte-related genes could be potential direct targets for *Suv420h2*by comparing H4K20me3 level at the promoters of several genes in iWAT during postnatal development. However, we did not observe differences in H4K20me3 levels at the promoters of *Ucp1* (**Supplemental Figure 21A**), RB transcriptional corepressor 1 (*Rb1)* (**Supplemental Figure 21B**), a negative regulator of brown adipocyte thermogenesis (41), and Krupple-like transcription factor 2 (*Klf2*) (**Supplemental Figure 21C**), a negative regulator of adipogenesis (42), in iWAT along the postnatal developmental course..

Suv420h2 is important in regulation of diet-induced obesity

To determine the role of *Suv420h2* in diet-induced obesity, we challenged H2KO, AH2Tg, and their respective WT littermates with a high fat diet (HFD). When housed at ambient room temperature (20-22ºC), H2KO mice had increased fat mass in iWAT and eWAT despite no change in body weight (**Supplemental Figure 22A-B**). This was associated with decreased energy expenditure in H2KO mice evident by reduced oxygen consumption and heat production (**Supplemental Figure 22C-D**) without changes in locomotor activity (**Supplemental Figure 22E**) and food intake (**Supplemental Figure 22F**).

Similarly, while there was no change in body weight (**Supplemental Figure 23A**), HFD-challenged AH2Tg mice housed at ambient room temperature had decreased fat mass in eWAT without changes in other fat pads (**Supplemental Figure 23B**). Ah2Tg mice also exhibited increased energy expenditure as shown by increased oxygen consumption and heat production (**Supplemental Figure 23C-D**) without changes locomotor activity (**Supplemental Figure 23E**) and food intake (**Supplemental Figure 23F**).

We previously reported that mild cold stress under ambient room temperature (20-22ºC) may trigger non-shivering thermogenesis (43). Thus, we also conducted HFD feeding experiments under thermoneutrality (30ºC).

When housed under thermoneutrality, H2KO mice gained more weight starting after 4 weeks of HFD feeding (**Figure 10A**) with increased fat mass in iBAT, iWAT and rWAT depots (**Figure 10B**), . and exhibited glucose intolerance and insulin resistance assessed by GTT and ITT, respectively (**Figure 10C-D**). In contrast, HFD-challenged AH2Tg mice gained less weight under thermoneutrality with lower fat mass in iBAT, iWAT and rWAT (**Figure 10E-F**), and exhibited improved glucose tolerance and insulin sensitivity as shown by GTT and ITT (**Figure 10G-H**). Thus, our data indicate that *Suv420h2* is important in regulating diet-induced obesity.

Discussion

Xue et al previously discovered developmentally induced beige adipocytes (14). To identify functional epigenetic marks that regulate brown/beige adipocyte development, we surveyed the expression of epigenetic enzymes responsible for histone modifications during the postnatal development of beige adipocytes and discovered a unique expression pattern of the histone methyltransferase *Suv420h2*, which mirrors that of *Ucp1*. Using genetic models with gain or loss of functions of *Suv420h2*, we demonstrate that *Suv420h2* promotes the development of brown and beige adipocytes postnatally, enhances cold-induced thermogenesis and prevents diet-induced obesity.

Methylation of H4K20 was one of the first histone modifications to be discovered, and is evolutionarily conserved from yeast to humans (17, 18). H4K20 can be mono-, di- and trimethylated (17, 18). SET8/PR-SET7 is the only known monomethyltransferase; whereas SUV420H1 and SUV420H2 are responsible for the di- and trimethylation of H4K20 (17, 18). The methylation states of H4K20 exert different biological function. Whereas H4K20me1 and H4K20me2 are involved in DNA replication and DNA damage repair, respectively, H4K20me3 is a hallmark of silenced heterochromatic regions and is also enriched in chromatin regions that contain silenced genes (17, 18, 44). H4K20me3 plays an important role in dynamic biological functions, including development, cellular differentiation, aging and cancer development (45-49). Here we demonstrate that H4K20me3, catalyzed by SUV420H2, may also be involved in the regulation of brown/beige fat thermogenesis and energy metabolism though 4E-BP1-PGC1α axis.

The enrichment of genes involved in mitochondrial functions revealed by our RNA-seq analysis drew our attention to *Pgc1α*, a master regulator of mitochondrial biogenesis and thermogenesis (28). (29, 30, 50)It has been demonstrated that PGC1α protein translation can be regulated by the eukaryotic translation initiation

complex (31). The eukaryotic translation initiation factor 4F (eIF4F) complex is composed of eIF4E (mRNA m7GTP 5' cap-binding protein), eIF4G (a scaffolding protein), and eIF4A (an ATP-dependent RNA helicase) (51). Recognition of the mRNA 5' cap structure by eIF4E is a rate-limiting step in translational initiation, and is hence tightly regulated (52). The activity of eIF4E is regulated through interaction with the three inhibitory 4E-BPs, 4E-BP1, 2 and 3. The 4E-BPs compete with eIF4G for a shared binding site on eIF4E (53), thereby negatively regulating eIF4F complex formation and translation initiation. Cold exposure down-regulates 4E-BP1 expression in BAT, which is mediated through β3-adrenergic agonist stimulated signaling pathways (54). Importantly, deletion of 4E-BP1 in mice results in greater reduction of adiposity, increased energy expenditure, up-regulated *Ucp1* expression and beige adipocyte induction in WAT; this is primarily due to increased eIF4F complex formation, leading to increased PGC1α protein translation (31). Indeed, we discovered that *4e-bp1* promoter H4K20me3 level is increased in *Suv420h2* overexpressing adipocytes, leading to down-regulated *4e-bp1* expression and corresponding up-regulated PGC1α protein levels. The enhanced PGC1α protein levels may drive the mitochondrial biogenesis in *Suv420h2* overexpressing adipocytes, resulting in increased brown fat thermogenesis.

SUV420H2 catalyzes the deposition of trimethylation to histone H4k20, which in turn represses gene transcription (17, 18). In the current study, we observed that overexpressing *Suv420h2* increased, whereas *Suv420h2* knockout decreased thermogenic gene expression in brown adipocytes. Thus, we could reasonably predict that SUV420h2 may repress a putative negative regulator of thermogenesis, which in turn promotes thermogenesis. Indeed, we have measured H4K20me3 levels at the promoters of several positive regulators of thermogenesis, including *Pgc1α*, *Pparγ*, *Prdm16* and *Esrrg*, none of them showed any differences in promoter H4K20me3 level between H2KO and AH2Tg mice, suggesting they are not direct targets for *Suv420h2*. We have also measured H4K20me3 levels at the promoters of several negative regulators of thermogenesis in adipose tissues, including *4e-bp1*, *Twist1*, *Zfp423* and *Rb1*. Only *4e-bp1* fit our criteria with decreased promoter H4K20me3 mark in H2KO mice and reciprocally increased promoter H4K20me3 levels in AH2Tg mice. Future studies with ChIP-seq using *Suv420h2* or H4K20me3 antibodies is warranted to identify Suv420h2- or H4K20me3- target genes.

In the current study, we also identified PGC1α as one of the targets whose protein synthesis could be regulated by 4E-BP1-dependent regulation of the eukaryotic translation initiation eIF4F complex activity. In

addition, whereas *Esrrg* mRNA transcription may not be directly regulated by SUV420H2,our data suggest that ESRRG protein levels may be regulated by 4E-BP1-mediated regulation of the eukaryotic translation initiation eIF4F complex activity, similarly to that of PGC1α. Although 4E-BP1 may regulate the whole translational machinery, the specificity may be regulated in part by specific transcriptional factor complexes on each target genes. Thus, future experiments with ribosome profiling or Ribo-seq technologies (55, 56) could be performed to identify potential protein candidates that are dependent on SUV420H2/H4K20me3/4E-BP1-regulated cap-dependent protein translation.

Along the course of our study, there were two papers published studying the roles of SUV420H1/H2 proteins in brown/beige adipocyte thermogenesis. Pedrotti et al reported that deletion of both *Suv420h1* and Suv420*h2* in brown adipocytes increased brown fat thermogenesis and ameliorated obesity via activating *Pparγ* regulated gene networks (21). The results were opposite to what we observed in our genetic models. The exact reason for this discrepancy is not clear. However, different genetic models were used in these two studies. For our purpose to distinguish the functions of *Suv420h2* from that of *Suv420h1*, we used animal models with *Suv420h2* deletion without affecting the expression of *Suv420h1*, whereas Pedrotti et al used animal models with *Suv420h1/Suv420h2* double deletion. Interestingly, we observed that either *Suv420h2* deletion or *Suv420h1* overexpression suppressed brown adipocyte thermogenic gene expression, suggesting that whereas *Suv420h2* may positively regulate brown adipocyte thermogenesis, *Suv420h1* may serve as a potential negative regulator. Thus, one possible reason accounting for the differences between our mouse models and those published by Pedrotti et al (21) is that deletion of *Suv420h1* in the *Suv420h1* and *Suv420h2* double knockout mouse model may dominate the phenotypes, thus resulting in increased mitochondrial function and thermogenesis in brown adipocytes; whereas in our animal model of *Suv420h2* deletion, reduced *Suv420h2* function along with normal or possibly enhanced *Suv420h1* function could collectively lead to impaired brown/beige adipocyte thermogenesis. Future studies using genetic models with gain- and loss-functions of individual Suv420h proteins are warranted to carefully dissect the effect of *Suv420hs* on adaptive thermogenesis.

Zhao et al (57) reported that mice with adipocyte-specific *Suv420h2/*lysine methyltransferase 5C *(Kmt5c)* deletion exerted decreased thermogenic gene expression in WAT and BAT, and were prone to diet-induced obesity and associated metabolic disorders, which was. similar to the phenotypes observed in our H2KO models. Mechanistically, the authors showed that enhanced expression of a negative regulator of brown fat

thermogenesis, transformation related protein 53 (*Trp53*) in *Suv420h2/Kmt5c* knockout (KO) mice, due to decreased H4K20me3 on its proximal promoter, was responsible for the metabolic phenotypes (57). In our current study, we have identified a new mechanism, in which *Suv420h2* suppresses the expression of a negative regulator of PGC1α protein translation, *4e-bp1*, by increasing repressive mark H4K20me3 on its promoter, thus promoting brown/beige adipocyte mitochondrial oxidative metabolism and thermogenesis. These complementary studies could significantly enhance our understandings of how *Suv420h1/h2* regulates brown/beige adipocyte thermogenesis and whole body metabolic homeostasis.

In our current study, we observed significant differences in the metabolic phenotypes in our animal models during a cold challenge, whereas the differences diminished in animals challenged with an obesogenic HFD at ambient temperature. It is possible that diet-induced thermogenesis and cold-induced thermogenesis may be triggered by different stimulations. In the context of increased energy needs (cold environment), the purpose of BAT activation is to increase heat production and maintain temperature stability. This is in contrast to a positive energy balance in diet-induced obesity, in which increased heat is not necessary, but energy expenditure increases owing to diet-induced thermogenesis, a phenomenon in which excess caloric consumption increases metabolic rate and stimulates BAT thermogenesis (2). Thermogenesis might be stimulated via different mechanisms, depending on whether it is triggered through cold or other factors (58). Additionally, cold and diet can lead to differential gene expression patterns in brown and white adipose tissue (59). Our previous data also showed that BAT responded differently in response to a HFD or a cold challenge (60). Thus, it is possible that there are differences in metabolic phenotypes in our animal model during a cold challenge vs a HFD challenge.

We also observed that metabolic differences during a HFD challenge was more evident in animals housed under thermoneutrality compared to the ambient temperature. Mice housed at ambient room temperature have a metabolic rate and food intake around 1.5 times higher than mice housed at thermoneutrality (3). While diet-induced thermogenesis might be primarily dependent on UCP1-dependent brown fat thermogenesis, metabolic rate in response to a cold environment could be influenced by factors other than brown fat adaptive thermogenesis, for example, shivering, skin/fur insulation, and most importantly, adipose tissue response to sympathetic activation (3, 61). These factors could mask the true intrinsic energetic demands in response to a high fat diet if mice are housed at ambient temperature that presents mild cold stress condition, which may be

partly responsible for the differences in metabolic phenotypes observed in our animal models housed at different environmental temperatures. The thermogenic adaptation to diet-induce obesity in an animal model may be partially dependent on the difference in environment temperature.

In summary, we discovered a unique expression pattern of the histone methyltransferase *Suv420h2*, which mirrors the appearance of developmental beige adipocytes. Using genetic models with loss- or gain-of-functions of *Suv420h2*, we demonstrate that *Suv420h2* promotes the development of brown and beige adipocytes postnatally, enhances cold-induced thermogenesis and prevents diet-induced obesity, possibly through 4E-BP1-PGC1α axis. We conclude that *Suv420h2* is a key regulator of brown/beige fat thermogenesis, energy metabolism and diet-induced obesity.

Materials and Methods

Sex as a biological variant. Our study examined both male and female mice. However, we found there was a sex-dimorphic effects and the phenotypes were more profound in males. Thus, results from male mice were reported.

Mice. Mice with whole body *Suv420h2* knockout (H2KO) were kindly provided by Dr. Gunnar Schotta (Ludwig Maximilian University, Munich, Germany)(22). To generate transgenic mice with adipocyte-specific *Suv420h2* overexpression (AH2Tg), a bacterial artificial chromosome (BAC) containing the mouse adiponectin gene was used, and full-length coding sequence of the mouse *Suv420h2* gene was PCR-amplified and inserted into the ATG position at exon 2 of the adiponectin gene in the BAC using homologous recombination. The adiponectin BAC carrying *Suv420h2* was linearized and microinjected into pronuclei of fertilized embryos of C57BL/6J mice at Georgia State University transgenic core facility.

Metabolic analysis. Mice were housed in a temperature- and humidity-controlled environment with a 12/12-hour light–dark cycle and had *ad libitum* access to water and food. H2KO, AH2Tg mice and their respective littermate controls were fed a regular chow diet (LabDiet 5001, LabDiet, St. Louis, MO, 13.5% calories from fat) or a HFD (Research Diets D12492, 60% calorie from fat) diet for up to 24 weeks. Various metabolic measurements were characterized. Body weight was monitored weekly. Body composition including fat and lean mass was analyzed using a Minispec NMR body composition analyzer (Bruker BioSpin Corporation; Billerica, MA). Food intake was measured in single-housed animals over seven consecutive days. Energy expenditure

and locomotor activity were assessed using PhenoMaster metabolic cage systems (TSE Systems, Chesterfield, MO). Insulin sensitivity was assessed by GTT and ITT, respectively(62, 63). Blood glucose was measured by OneTouch Ultra Glucose meter (LifeScan, Milpitas, CA). At the end of experiments, tissues including BAT and WAT were dissected, weighed, and frozen in liquid nitrogen for further analysis.

Cold exposure. H2KO, AH2Tg mice and their respective littermate controls were subjected to a cold challenge (5-6°C) for 7 days. To measure body temperature, some animals were surgically implanted with a temperature transponder (BioMedic Data Systems, Seaford, DE) in the peritoneal cavity (62, 63). At the end of experiment, WAT and BAT were dissected, weighed and frozen for further analysis.

Cell culture and SiRNA knockdown. Immortalized BAT1 brown adipocyte cells (15, 16) were kindly provided by Dr. Patrick Seale (University of Pennsylvania, Philadelphia, PA). BAT1 brown adipocytes were grown and differentiated as we described (63). *Suv420h2, 4e-bp1* targeting siRNA, and non-targeting scramble siRNAwere purchased from Dharmacon (Lafayette, CO) (**Supplemental Table 1**).Plasmids containing *Suv420h1* and *Suv420h2* cDNAs were purchased from Open Biosystems (Huntsville, AL) (**Supplemental Table 1**). *Suv420h2, 4e-bp1* siRNAs, or *Suv420h1* or *Suv420h2* overexpression plasmids were electroporated into BAT1 brown adipocytes using Amaxa Nucleofector II Electroporator (Lonza) with an Amaxa cell line nucleofector kit L (Lonza) (63). In some experiments, after *Suv420h2* siRNAs knockdown, BAT1 cells were further treated with the SUV420H1/H2 inhibitor A196 (5μM) (Sigma-Aldrich, St. Louis, MO, catalog #SML1565) (19) for an additional 24 hours. In other experiments, BAT1 brown adipocytes were treated with both *Suv420h2* and *4e-bp1* siRNAs to knockdown both *Suv420h2* and *4e-bp1*. Some cells were also treated with either vehicle (PBS) or the adrenergic agonist norepinephrine (1μm) for 4 hours.

Quantitative RT-PCR analysis of gene expression. Total RNA was extracted from fat tissues using Tri Reagent kit (Molecular Research Center, Cincinnati, OH) (62, 63). The expression of target genes was measured by quantitative RT-PCR analysis with a TaqMan Universal PCR Master Mix kit (ThermoFisher Scientific, Waltham, MA) using an Applied Biosystems QuantStudio 3 real-time PCR system (ThermoFisher Scientific) (62, 63). The TaqMan primers/probe pairs for the gene expression measurements were either purchased from Applied Biosystems (ThermoFisher Scientific) (**Supplemental Table 2**) or commercially synthesized (Applied Biosystems, the sequences were listed in **Supplemental Table 3**).

Immunoblotting. Protein levels of target genes were measured by immunoblotting as we described (62, 63). Briefly, fat tissues were disrupted with a homogenizer in a modified radioimmunoprecipitation assay (RIPA) lysis buffer supplemented with protease and phosphatase inhibitor mixtures (Sigma-Aldrich, St. Louis, MO). After centrifugation, supernatants were resolved by SDS-PAGE, and transferred to nitrocellulose membranes (Bio-Rad, Hercules, CA), followed by incubating with various primary antibodies and Alexa Fluor 680-conjugated secondary antibodies (Life Science Techenologies). The blots were developed with a Li-COR Imager System (Li-COR Biosciences, Lincoln, NE). The antibody information was listed in **Supplemental Table 4**.

Immunohistochemistry (IHC). IHC was conducted as we described(62, 63). Briefly, fat tissues were fixed in neutral formalin, embedded in paraffin and sliced into 5 μm sections. The tissue slides were used for hematoxylin and eosin (H&E) staining, or immunochemical-staining with primary and secondary antibodies, which were further developed with an alkaline phosphatase substrate using Vector Red Substrate kit (Vector Laboratories, SK-5100). Histological images were captured using an Olympus DP73 photomicroscope and CellSens software (Olympus, Waltham, MA). The adipocyte size was measured using ImageJ software with Adiposoft plug-in (64). The primary and secondary antibodies are listed in **Supplemental Table 4**.

Chromatin immunoprecipitation (ChIP) assays. ChIP assays were performed with a ChIP assay kit (Upstate BioTechnology, Lake Placid, NY) as we described (63). Briefly, fat tissues were fixed and dounce-homogenized for nuclei isolation. The nuclei were used for sonication to shear DNA, followed by immunoprecipitation and elution. The immunoprecipitated DNA was quantitated by real-time PCR using SYBR green. The information for primer sequences was shown in **Supplemental Table 5**.

Oxygen consumption rate (OCR) measurement. Brown adipocyte OCR was measured using a XF 96 Extracellular Flux Analyzer (Agilent, Santa Clara, CA) as we described (63). OCR measurement began with a basal respiration recording, followed by addition of other reagents including oligomycin for inhibition of the coupled respiration and FCCP for maximal respiration.

RNAseq analysis. Total RNA was isolated from iWAT of cold-challenged WT, H2KO and AH2Tg mice. Equal amount of RNA from 6 animals/group was pooled and sent to Beijing Genomics Institute (BGI, Shenzhen, China) for RNAseq analysis.. Clean reads were aligned to the mouse reference genome (University of California Santa Cruz Mouse Genome Browser mm9 Assembly) using SOAPaligner/SOAP2 (65). Differential expression analysis was performed using DESeq2 (66). Differentially expressed genes between groups were defined as

Log2 fold change cutoff threshold of 0.5 and false discovery rate (FDR)<0.05. Pathway analysis was performed using the clusterProfiler (67). The RNAseq data was also used to predict adipose tissue browning capacity with an online bioinformatic software (https://github.com/PerocchiLab/ProFAT) (23).

Assay for transposase-accessible chromatin sequencing (ATAC-seq) analysis. ATAC-seq was conducted according to the Omni-ATAC-seq protocol as described (68). Briefly, BAT tissues were dounce-homogenized, filtered and centrifuged in iodixanol solution to obtain nuclei. The nuclei were treated with Nextera Tn5 transposase (Illumina, San Diego, CA) for the transposition reaction, followed by DNA purification and PCR amplification with NEBNext 2X MasterMix (New England BioLabs, Ipswich, MA) and Nextera Index primers (Illumina). The ATAC libraries were further size-purified and sent to Novogene (Durham, NC) for sequencing. The ATAC-seq analysis was performed on the Galaxy server as described(68). Briefly, the adaptor-trimmed sequencing reads were mapped to the mm10 mouse reference genome using Bowtie2 (69). After removing PCR duplicates and reads mapped to ENCODE blacklist regions, the ATAC-seq peaks were called using MACS2 (70). Finally, differential ATAC-seq peaks between groups were identified using DiffBind. The integration of RNA-seq and ATAC-seq data was carried out in R, and heatmaps were generated using the ComplexHeatmap package (71).

Statistical analysis. Data were expressed as mean ±SEM. Statistical tests were performed using SPSS software (version 16.0, SPSS Inc, Chicago, IL, USA). Differences between groups were analyzed for statistical significance by Student's t-test, one-way or two-way ANOVA, or two-way ANOVA with repeated measures as appropriate. Statistical significance was accepted at $p<0.05$.

Study Approval. All animal procedures conducted in the study were approved by the Institutional Animal Care and Use Committee (IACUC) at Georgia State University (GSU).

Data availability. The RNA-seq and ATAC-seq data have been deposited to Gene Expression Omnibus (GEO) database with the accession code GSE244457 and GSE245509, respectively. Values for graphs in the Figureures and Supplemental Figureures are provided in the Supporting Data Values file.

Acknowlegements. This work is supported by NIH grants R01DK107544, R01DK118106 and R01DK125081, and American Diabetes Association (ADA) grant 1-18-IBS-260to BX; NIH grants R01DK115740, R01DK118106,

and ADA grant 1-18-19 IBS-348 to HS; NIH grants R01DK111052, DK116496, and ADA grant 1-18-IBS-346 to LY.

Author Contributions. XC performed most of the experiments and analyzed the data; QC, FL, JJ, ZL, and XY assisted with various experiments; HDS performed bioinformatic analysis of RNAseq and ATACseq data; GS and LY contributed to conceptual and technical inputs and review/edits on manuscript; HS and BZ conceived and designed the study and wrote the manuscript.

Declaration of Interest. The authors declare no conflict of interests.

References.

1. Lowell BB, and Spiegelman BM. Towards a molecular understanding of adaptive thermogenesis. *Nature.* 2000;404(6778):652-60.
2. Cannon B, and Nedergaard J. Brown adipose tissue: function and physiological significance. *Physiol Rev.* 2004;84(1):277-359.
3. Cannon B, and Nedergaard J. Nonshivering thermogenesis and its adequate measurement in metabolic studies. *J Exp Biol.* 2011;214(Pt 2):242-53.
4. Kazak L, Chouchani ET, Jedrychowski MP, Erickson BK, Shinoda K, Cohen P, et al. A creatine-driven substrate cycle enhances energy expenditure and thermogenesis in beige fat. *Cell.* 2015;163(3):643-55.
5. Ikeda K, Kang Q, Yoneshiro T, Camporez JP, Maki H, Homma M, et al. UCP1-independent signaling involving SERCA2b-mediated calcium cycling regulates beige fat thermogenesis and systemic glucose homeostasis. *Nat Med.* 2017;23(12):1454-65.
6. Cinti S. The adipose organ. *Prostaglandins Leukot Essent Fatty Acids.* 2005;73(1):9-15.
7. Petrovic N, Walden TB, Shabalina IG, Timmons JA, Cannon B, and Nedergaard J. Chronic peroxisome proliferator-activated receptor gamma (PPARgamma) activation of epididymally derived white adipocyte cultures reveals a population of thermogenically competent, UCP1-containing adipocytes molecularly distinct from classic brown adipocytes. *J Biol Chem.* 2010;285(10):7153-64.
8. Wu J, Bostrom P, Sparks LM, Ye L, Choi JH, Giang AH, et al. Beige adipocytes are a distinct type of thermogenic fat cell in mouse and human. *Cell.* 2012;150(2):366-76.
9. Himms-Hagen J, Cui J, Danforth E, Jr., Taatjes DJ, Lang SS, Waters BL, et al. Effect of CL-316,243, a thermogenic beta 3-agonist, on energy balance and brown and white adipose tissues in rats. *Am J Physiol.* 1994;266(4 Pt 2):R1371-82.
10. Kopecky J, Clarke G, Enerback S, Spiegelman B, and Kozak LP. Expression of the mitochondrial uncoupling protein gene from the aP2 gene promoter prevents genetic obesity. *J Clin Invest.* 1995;96(6):2914-23.
11. Cypess AM, Lehman S, Williams G, Tal I, Rodman D, Goldfine AB, et al. Identification and importance of brown adipose tissue in adult humans. *N Engl J Med.* 2009;360(15):1509-17.
12. van Marken Lichtenbelt WD, Vanhommerig JW, Smulders NM, Drossaerts JM, Kemerink GJ, Bouvy ND, et al. Cold-activated brown adipose tissue in healthy men. *N Engl J Med.* 2009;360(15):1500-8.
13. Virtanen KA, Lidell ME, Orava J, Heglind M, Westergren R, Niemi T, et al. Functional brown adipose tissue in healthy adults. *N Engl J Med.* 2009;360(15):1518-25.
14. Xue B, Rim JS, Hogan JC, Coulter AA, Koza RA, and Kozak LP. Genetic variability affects the development of brown adipocytes in white fat but not in interscapular brown fat. *J Lipid Res.* 2007;48(1):41-51.
15. Rajakumari S, Wu J, Ishibashi J, Lim HW, Giang AH, Won KJ, et al. EBF2 determines and maintains brown adipocyte identity. *Cell Metab.* 2013;17(4):562-74.
16. Seale P, Kajimura S, Yang W, Chin S, Rohas LM, Uldry M, et al. Transcriptional control of brown fat determination by PRDM16. *Cell Metab.* 2007;6(1):38-54.

17. Jorgensen S, Schotta G, and Sorensen CS. Histone H4 lysine 20 methylation: key player in epigenetic regulation of genomic integrity. *Nucleic Acids Res.* 2013;41(5):2797-806.
18. Schotta G, Lachner M, Sarma K, Ebert A, Sengupta R, Reuter G, et al. A silencing pathway to induce H3-K9 and H4-K20 trimethylation at constitutive heterochromatin. *Genes Dev.* 2004;18(11):1251-62.
19. Bromberg KD, Mitchell TR, Upadhyay AK, Jakob CG, Jhala MA, Comess KM, et al. The SUV4-20 inhibitor A-196 verifies a role for epigenetics in genomic integrity. *Nat Chem Biol.* 2017;13(3):317-24.
20. Moffat C, Bhatia L, Nguyen T, Lynch P, Wang M, Wang D, et al. Acyl-CoA thioesterase-2 facilitates mitochondrial fatty acid oxidation in the liver. *J Lipid Res.* 2014;55(12):2458-70.
21. Pedrotti S, Caccia R, Neguembor MV, Garcia-Manteiga JM, Ferri G, de Palma C, et al. The Suv420h histone methyltransferases regulate PPAR-gamma and energy expenditure in response to environmental stimuli. *Sci Adv.* 2019;5(4):eaav1472.
22. Schotta G, Sengupta R, Kubicek S, Malin S, Kauer M, Callen E, et al. A chromatin-wide transition to H4K20 monomethylation impairs genome integrity and programmed DNA rearrangements in the mouse. *Genes Dev.* 2008;22(15):2048-61.
23. Cheng Y, Jiang L, Keipert S, Zhang S, Hauser A, Graf E, et al. Prediction of Adipose Browning Capacity by Systematic Integration of Transcriptional Profiles. *Cell Rep.* 2018;23(10):3112-25.
24. Kraus D, Yang Q, Kong D, Banks AS, Zhang L, Rodgers JT, et al. Nicotinamide N-methyltransferase knockdown protects against diet-induced obesity. *Nature.* 2014;508(7495):258-62.
25. Neinast MD, Frank AP, Zechner JF, Li Q, Vishvanath L, Palmer BF, et al. Activation of natriuretic peptides and the sympathetic nervous system following Roux-en-Y gastric bypass is associated with gonadal adipose tissues browning. *Mol Metab.* 2015;4(5):427-36.
26. Pan D, Fujimoto M, Lopes A, and Wang YX. Twist-1 is a PPARdelta-inducible, negative-feedback regulator of PGC-1alpha in brown fat metabolism. *Cell.* 2009;137(1):73-86.
27. Shao M, Ishibashi J, Kusminski CM, Wang QA, Hepler C, Vishvanath L, et al. Zfp423 Maintains White Adipocyte Identity through Suppression of the Beige Cell Thermogenic Gene Program. *Cell Metab.* 2016;23(6):1167-84.
28. Puigserver P, Wu Z, Park CW, Graves R, Wright M, and Spiegelman BM. A cold-inducible coactivator of nuclear receptors linked to adaptive thermogenesis. *Cell.* 1998;92(6):829-39.
29. Olson BL, Hock MB, Ekholm-Reed S, Wohlschlegel JA, Dev KK, Kralli A, et al. SCFCdc4 acts antagonistically to the PGC-1alpha transcriptional coactivator by targeting it for ubiquitin-mediated proteolysis. *Genes Dev.* 2008;22(2):252-64.
30. Wei P, Pan D, Mao C, and Wang YX. RNF34 is a cold-regulated E3 ubiquitin ligase for PGC-1alpha and modulates brown fat cell metabolism. *Mol Cell Biol.* 2012;32(2):266-75.
31. Tsukiyama-Kohara K, Poulin F, Kohara M, DeMaria CT, Cheng A, Wu Z, et al. Adipose tissue reduction in mice lacking the translational inhibitor 4E-BP1. *Nat Med.* 2001;7(10):1128-32.
32. Azar R, Lasfargues C, Bousquet C, and Pyronnet S. Contribution of HIF-1alpha in 4E-BP1 gene expression. *Mol Cancer Res.* 2013;11(1):54-61.
33. Azar R, Najib S, Lahlou H, Susini C, and Pyronnet S. Phosphatidylinositol 3-kinase-dependent transcriptional silencing of the translational repressor 4E-BP1. *Cell Mol Life Sci.* 2008;65(19):3110-7.
34. Stephenson AH, Christian JF, and Seidel ER. Polyamines regulate eukaryotic initiation factor 4E-binding protein 1 gene transcription. *Biochem Biophys Res Commun.* 2004;323(1):204-12.
35. Bargut TC, Aguila MB, and Mandarim-de-Lacerda CA. Brown adipose tissue: Updates in cellular and molecular biology. *Tissue Cell.* 2016;48(5):452-60.
36. Nedergaard J, Petrovic N, Lindgren EM, Jacobsson A, and Cannon B. PPARgamma in the control of brown adipocyte differentiation. *Biochim Biophys Acta.* 2005;1740(2):293-304.
37. Seale P, Bjork B, Yang W, Kajimura S, Chin S, Kuang S, et al. PRDM16 controls a brown fat/skeletal muscle switch. *Nature.* 2008;454(7207):961-7.
38. Shao M, Zhang Q, Truong A, Shan B, Vishvanath L, Li L, et al. ZFP423 controls EBF2 coactivator recruitment and PPARgamma occupancy to determine the thermogenic plasticity of adipocytes. *Genes Dev.* 2021;35(21-22):1461-74.
39. Ahmadian M, Liu S, Reilly SM, Hah N, Fan W, Yoshihara E, et al. ERRgamma Preserves Brown Fat Innate Thermogenic Activity. *Cell Rep.* 2018;22(11):2849-59.
40. Muller S, Perdikari A, Dapito DH, Sun W, Wollscheid B, Balaz M, et al. ESRRG and PERM1 Govern Mitochondrial Conversion in Brite/Beige Adipocyte Formation. *Front Endocrinol (Lausanne).* 2020;11:387.

41. Scime A, Grenier G, Huh MS, Gillespie MA, Bevilacqua L, Harper ME, et al. Rb and p107 regulate preadipocyte differentiation into white versus brown fat through repression of PGC-1alpha. *Cell Metab.* 2005;2(5):283-95.
42. Banerjee SS, Feinberg MW, Watanabe M, Gray S, Haspel RL, Denkinger DJ, et al. The Kruppel-like factor KLF2 inhibits peroxisome proliferator-activated receptor-gamma expression and adipogenesis. *J Biol Chem.* 2003;278(4):2581-4.
43. Cui X, Nguyen NL, Zarebidaki E, Cao Q, Li F, Zha L, et al. Thermoneutrality decreases thermogenic program and promotes adiposity in high-fat diet-fed mice. *Physiol Rep.* 2016;4(10).
44. Balakrishnan L, and Milavetz B. Decoding the histone H4 lysine 20 methylation mark. *Crit Rev Biochem Mol Biol.* 2010;45(5):440-52.
45. Biron VL, McManus KJ, Hu N, Hendzel MJ, and Underhill DA. Distinct dynamics and distribution of histone methyl-lysine derivatives in mouse development. *Dev Biol.* 2004;276(2):337-51.
46. Kwon MJ, Kim SS, Choi YL, Jung HS, Balch C, Kim SH, et al. Derepression of CLDN3 and CLDN4 during ovarian tumorigenesis is associated with loss of repressive histone modifications. *Carcinogenesis.* 2010;31(6):974-83.
47. Pogribny IP, Tryndyak VP, Muskhelishvili L, Rusyn I, and Ross SA. Methyl deficiency, alterations in global histone modifications, and carcinogenesis. *J Nutr.* 2007;137(1 Suppl):216S-22S.
48. Sarg B, Koutzamani E, Helliger W, Rundquist I, and Lindner HH. Postsynthetic trimethylation of histone H4 at lysine 20 in mammalian tissues is associated with aging. *J Biol Chem.* 2002;277(42):39195-201.
49. Tsang LW, Hu N, and Underhill DA. Comparative analyses of SUV420H1 isoforms and SUV420H2 reveal differences in their cellular localization and effects on myogenic differentiation. *PLoS One.* 2010;5(12):e14447.
50. Clarke KJ, Adams AE, Manzke LH, Pearson TW, Borchers CH, and Porter RK. A role for ubiquitinylation and the cytosolic proteasome in turnover of mitochondrial uncoupling protein 1 (UCP1). *Biochim Biophys Acta.* 2012;1817(10):1759-67.
51. Gingras AC, Raught B, and Sonenberg N. eIF4 initiation factors: effectors of mRNA recruitment to ribosomes and regulators of translation. *Annu Rev Biochem.* 1999;68:913-63.
52. Pause A, Belsham GJ, Gingras AC, Donze O, Lin TA, Lawrence JC, Jr., et al. Insulin-dependent stimulation of protein synthesis by phosphorylation of a regulator of 5'-cap function. *Nature.* 1994;371(6500):762-7.
53. Haghighat A, Mader S, Pause A, and Sonenberg N. Repression of cap-dependent translation by 4E-binding protein 1: competition with p220 for binding to eukaryotic initiation factor-4E. *EMBO J.* 1995;14(22):5701-9.
54. Lehr L, Kuehne F, Arboit P, Giacobino JP, Poulin F, Muzzin P, et al. Control of 4E-BP1 expression in mouse brown adipose tissue by the beta3-adrenoceptor. *FEBS Lett.* 2004;576(1-2):179-82.
55. Ingolia NT, Brar GA, Rouskin S, McGeachy AM, and Weissman JS. The ribosome profiling strategy for monitoring translation in vivo by deep sequencing of ribosome-protected mRNA fragments. *Nat Protoc.* 2012;7(8):1534-50.
56. Ingolia NT, Ghaemmaghami S, Newman JR, and Weissman JS. Genome-wide analysis in vivo of translation with nucleotide resolution using ribosome profiling. *Science.* 2009;324(5924):218-23.
57. Zhao Q, Zhang Z, Rong W, Jin W, Yan L, Jin W, et al. KMT5c modulates adipocyte thermogenesis by regulating Trp53 expression. *Proc Natl Acad Sci U S A.* 2020;117(36):22413-22.
58. Peterson CM, Lecoultre V, Frost EA, Simmons J, Redman LM, and Ravussin E. The thermogenic responses to overfeeding and cold are differentially regulated. *Obesity (Silver Spring).* 2016;24(1):96-101.
59. Hansen IR, Jansson KM, Cannon B, and Nedergaard J. Contrasting effects of cold acclimation versus obesogenic diets on chemerin gene expression in brown and brite adipose tissues. *Biochim Biophys Acta.* 2014;1841(12):1691-9.
60. Bruggeman EC, Garretson JT, Wu R, Shi H, and Xue B. Neuronal Dnmt1 Deficiency Attenuates Diet-Induced Obesity in Mice. *Endocrinology.* 2018;159(1):145-62.
61. Feldmann HM, Golozoubova V, Cannon B, and Nedergaard J. UCP1 ablation induces obesity and abolishes diet-induced thermogenesis in mice exempt from thermal stress by living at thermoneutrality. *Cell Metab.* 2009;9(2):203-9.
62. Cui X, Jing J, Wu R, Cao Q, Li F, Li K, et al. Adipose tissue-derived neurotrophic factor 3 regulates sympathetic innervation and thermogenesis in adipose tissue. *Nat Commun.* 2021;12(1):5362.
63. Li F, Jing J, Movahed M, Cui X, Cao Q, Wu R, et al. Epigenetic interaction between UTX and DNMT1 regulates diet-induced myogenic remodeling in brown fat. *Nat Commun.* 2021;12(1):6838.
64. Galarraga M, Campion J, Munoz-Barrutia A, Boque N, Moreno H, Martinez JA, et al. Adiposoft: automated software for the analysis of white adipose tissue cellularity in histological sections. *J Lipid Res.* 2012;53(12):2791-6.

65. Li R, Yu C, Li Y, Lam TW, Yiu SM, Kristiansen K, et al. SOAP2: an improved ultrafast tool for short read alignment. *Bioinformatics.* 2009;25(15):1966-7.
66. Love MI, Huber W, and Anders S. Moderated estimation of fold change and dispersion for RNA-seq data with DESeq2. *Genome Biol.* 2014;15(12):550.
67. Wu T, Hu E, Xu S, Chen M, Guo P, Dai Z, et al. clusterProfiler 4.0: A universal enrichment tool for interpreting omics data. *Innovation (Camb).* 2021;2(3):100141.
68. Ding ZC, Shi H, Aboelella NS, Fesenkova K, Park EJ, Liu Z, et al. Persistent STAT5 activation reprograms the epigenetic landscape in CD4(+) T cells to drive polyfunctionality and antitumor immunity. *Sci Immunol.* 2020;5(52).
69. Langmead B, and Salzberg SL. Fast gapped-read alignment with Bowtie 2. *Nat Methods.* 2012;9(4):357-9.
70. Zhang Y, Liu T, Meyer CA, Eeckhoute J, Johnson DS, Bernstein BE, et al. Model-based analysis of ChIP-Seq (MACS). *Genome Biol.* 2008;9(9):R137.
71. Gu Z, Eils R, and Schlesner M. Complex heatmaps reveal patterns and correlations in multidimensional genomic data. *Bioinformatics.* 2016;32(18):2847-9.

Figure Legends.

Figure 1. *Suv420h2* is important in regulating Ucp1 expression.

(A)-(B) The expression of *Ucp1* (A) and *Suv420h2* (B) in iWAT of male C57BL/6J mice during postnatal development, n=4 for postnatal days 10 and 60, and n=5 for postnatal days 15, 20 and 30. *p<0.05 by one-way ANOVA followed by Tukey's multiple comparisons test.

(C) The expression of *Suv420h2* in brown and white adipose tissues in 2-3 months old male C57BL/6J mice, n=4/group. *p<0.05 by one-way ANOVA followed by Tukey's multiple comparisons test.

(D)-(E) The expression of *Ucp1* (D) and *Suv420h2* (E) in iWAT of 2-3 months old male C57BL/6J mice during a 5°C cold exposure challenge, n=10 in (D) and n=4 in (E). *p<0.05 by one-way ANOVA followed by Tukey's multiple comparisons test.

(F)-(G) The expression of *Ucp1* (F) and *Suv420h2* (G) during BAT1 brown adipocyte differentiation, n=4-6/group. *p<0.05 by one-way ANOVA followed by Tukey's multiple comparisons test.

(H)-(I) H4K20 mono-, di- and tri-methylation levels in BAT1 brown adipocytes with scramble siRNA (Control) and *Suv420h2* (H2KD) siRNA knockdown (H) or with empty vector (Control) and *Suv420h2* (H2OE) overexpression (I), n=3/group. *p<0.05 by unpaired two-tailed Student's t-test. Blots were run in parallel at the same time.

(J)-(K) The expression of *Ucp1* in BAT1 brown adipocytes with *Suv420h2* knockdown (J) or *Suv420h2* overexpression (K), n=4-6/group. *p<0.05 by two-way ANOVA followed by Tukey's multiple comparisons test.

(L) The expression of *Ucp1* in BAT1 brown adipocytes with overexpression of either empty vector (Control) or *Suv420h1* (H1 OE), n=4-5/group. *p<0.05 by two-way ANOVA followed by Tukey's multiple comparisons test.

(M-O) The expression of *Ucp1* (M), *Dio2* (N) and *Acot2* (O) in BAT1 brown adipocytes with *Suv420h2* knockdown and further treated with either vehicle (dimethyl sulfoxide (DMSO)) or the SUV420H1/H2 inhibitor A196. Four-day differentiated BAT1 cells were treated with either scramble or *Suv420h2* siRNA via electroporation. On day 6 of differentiation, cells were further treated with either DMSO or the SUV420H1/H2 inhibitor A196 (5μM) for 24 hours. Before harvesting, cells were further treated with either PBS or NE (1μm) for 4 hours, n=3-4/group. Bars with a different letter indicate statistical significance at p<0.05 as analyzed by two-way ANOVA followed by Tukey's multiple comparisons test. Control: Scramble siRNA+DMSO; H2KD: *Suv420h2* siRNA+DMSO; H2KD+A196: *Suv420h2* siRNA+A196.

All data are expressed as mean ± SEM.

Figure 2. *Suv420h2* regulates the development of brown and beige fat.

(A) –(D) UCP1 protein levels (A), UCP1 immunostaining (B), H&E staining (C), and quantification of adipocyte size (D) in iBAT of 20-day-old H2KO and WT mice housed at room temperature. In (A), n=4-5/group. *p<0.05 vs. WT by unpaired two-tailed Student's t-test. In (B), images are representatives from 3 replicate animals/group. Images from additional animals can be found in Supplemental Figure 6A. Scale bar=70μm in (B) and (C). In (D), n=3/group. *p<0.05 as analyzed by two-way ANOVA followed by Tukey's multiple comparisons test.

(E) –(H) UCP1 protein levels (E), UCP1 immunostaining (F), H&E staining (G) and Quantification of adipocyte size (H) in iWAT of 20-day-old H2KO and WT mice housed at room temperature. In (E), n=3/group. *p<0.05 vs. WT by unpaired two-tailed Student's t-test. In (F), images are representatives from 3 replicate animals/group. Images from additional

animals can be found in Supplemental Figure 6B-C. Scale bar=140μm in (F) and (G). In (H), n=4/group. *p<0.05 as analyzed by two-way ANOVA followed by Tukey's multiple comparisons test.

(I) –(L) UCP1 protein levels (I), UCP1-immunostaining (J), H&E staining (K) and quantification of adipocyte size (L) in iBAT of 20-day-old AH2Tg and WT mice housed at room temperature. In (I), n=4-5/group. *p<0.05 vs. WT by unpaired two-tailed Student's t-test. In (J), images are representatives from 3 replicate animals/group). Images from additional animals can be found in Supplemental Figure 8A Scale bar=70μm in (J) and (K). In (L), n=3/group. *p<0.05 as analyzed by two-way ANOVA followed by Tukey's multiple comparisons test.

(M) –(P) UCP1 protein levels (M), UCP1-immunostaining (N), H&E staining (O) and Quantitation of adipocyte size (P) in iWAT of 20-day-old AH2Tg and WT mice housed at room temperature. In (M), n=3/group. *p<0.05 vs. WT by unpaired two-tailed Student's t-test. In (N), images are representatives from 3 replicate animals/group. Images from additional animals can be found in Supplemental Figure 8B-C. Scale bar=140μm in (N) and (O). In (P), n=3/group. *p<0.05 as analyzed by two-way ANOVA followed by Tukey's multiple comparisons test.

All data are expressed as mean ± SEM. UCP1-positive multilocular brown/beige adipocytes were shown in dark purplish red color, and were indicated with black arrows; and UCP1-negative unilocular white adipocytes were shown in light color, and were indicated with red arrows.

Figure 3. H2KO mice have impaired brown/beige adipocyte thermogenesis during a 7-day cold challenge. Three-month-old male H2KO and their WT littermates were challenged with a chronic 7-day cold at 5°C.

(A) –(B) Core body temperature (A) and fat pad weight (B) in WT and H2KO mice during the cold challenge. In (A), n=7 for WT and n=5 for H2KO. *p<0.05 by two-way ANOVA with repeated measures followed by Tukey's multiple comparisons test. In (B), n=5/group. *p<0.05 by unpaired two-tailed Student's t-test.

(C) –(D) H&E staining (C) and quantification of adipocyte size (D) in iBAT and iWAT of WT and H2KO mice after the 7-day cold exposure. In (C), scale bar=70μm for iBAT and 140μm for iWAT. In (D), n=3/group. *p<0.05 by two-way ANOVA followed by Tukey's multiple comparisons test.

(E)-(F) Gene expression analysis in iBAT (E) and iWAT (F) of WT and H2KO mice after the 7-day cold exposure, n=6/group in (E) and n=5/group in (F). *p<0.05 by unpaired two-tailed Student's t-test.

(G)-(H) UCP1 protein and H4K20me3 levels in iBAT (G) and iWAT (H) of WT and H2KO mice after the 7-day cold exposure, n=5 (WT), n=3 (H2KO) in (G) and n=4/group in (H). *p<0.05 by unpaired two-tailed Student's t-test.

(I) UCP1 immunostaining in iBAT and iWAT of WT and H2KO mice after the 7-day cold exposure (Representative images from 3 replicate animals/group). Images from additional animals can be found in Supplemental Figure 9A-C. UCP1-positive multilocular brown/beige adipocytes were shown in dark purplish red color, and were indicated with black arrows; and UCP1-negative unilocular white adipocytes were shown in light color, and were indicated with red arrows. Scale bar=70μm for iBAT and 140μm for iWAT.

(J) Oxygen consumption rate (OCR) in primary brown adipocytes isolated from iBAT of male WT and H2KO mice measured by a Seahorse XF 96 Extracellular Flux Analyzer, n=9 (WT) and 8 (H2KO). *p<0.05 by two-way ANOVA with repeated measures followed by Tukey's multiple comparisons test or by unpaired two-tailed Student's t-test.

All data are expressed as mean ± SEM.

Figure 4. AH2Tg mice have enhanced brown/beige adipocyte thermogenesis during a 7-day cold challenge. Three-month-old male AH2Tg and their WT littermates were challenged with a chronic 7-day cold at 5°C.

(A) –(B) Core body temperature (A) and fat pad weight (B) in WT and AH2Tg mice during the cold challenge. In (A), n=7 for WT and n=6 for H2KO. *p<0.05 by two-way ANOVA with repeated measures followed by Tukey's multiple comparisons test. In (B), n=7/group. *p<0.05 by unpaired two-tailed Student's t-test.

(C) –(D) H&E staining (C) and quantification of adipocyte size (D) in iBAT and iWAT of WT and AH2Tg mice after the 7-day cold exposure. In (C), scale bar=70μm for iBAT and 140μm for iWAT. In (D), n=3/group in iBAT and n=4/group in iWAT. *p<0.05 by two-way ANOVA followed by Tukey's multiple comparisons test.

(E)-(F) Gene expression analysis in iBAT (E) and iWAT (F) of WT and AH2Tg mice after the 7-day cold exposure, n=7/group in (E) and n=8/group in (F). *p<0.05 by unpaired two-tailed Student's t-test.

(G)-(H) UCP1 protein and H4K20me3 levels in iBAT (G) and iWAT (H) of WT and AH2Tg mice after the 7-day cold exposure, n=3/group. *p<0.05 by unpaired two-tailed Student's t-test.

(I) UCP1 immunostaining in iBAT and iWAT of WT and AH2Tg mice after the 7-day cold exposure (Representative images from 3 replicate animals/group). Images from additional animals can be found in Supplemental Figure 10A-C. UCP1-positive multilocular brown/beige adipocytes were shown in dark purplish red color, and were indicated with black arrows; and UCP1-negative unilocular white adipocytes were shown in light color, and were indicated with red arrows. Scale bar=70μm for iBAT and 140μm for iWAT.

(J) Oxygen consumption rate (OCR) in primary brown adipocytes isolated from iBAT of male WT and AH2Tg mice measured by a Seahorse XF 96 Extracellular Flux Analyzer, n=8 (WT) and 9 (H2KO). *p<0.05 by two-way ANOVA with repeated measures followed by Tukey's multiple comparisons test or by unpaired two-tailed Student's t-test.

All data are expressed as mean ± SEM.

Figure 5. SUV420H2 regulates mitochondrial bioenergetic program.

(A)-(B) RNAseq analysis of BAT-specific gene expression in iWAT of male H2KO mice (A) and male AH2Tg mice (B) after the 7-day cold exposure using an online software (https://github.com/PerocchiLab/ProFAT). The WAT reference aggregate and BAT reference aggregate were derived from the online software.

(C) Heatmaps of genes that are reciprocally regulated in iWAT of H2KO and AH2Tg mice after cold exposure.

(D) Analysis of pathways that are reciprocally regulated in iWAT of H2KO and AH2Tg mice after cold exposure.

(E) Comparison of genome-wide alterations in chromatin accessibility landscape assessed by ATAC-seq with the corresponding gene expression assessed by RNA-seq of AH2Tg and WT mice after the 7-day cold exposure.

Figure 6. SUV420H2 regulates mitochondrial respiratory chain complex protein levels.

(A)-(B) Immunoblotting of mitochondrial respiratory chain complex proteins in iBAT (A) and iWAT (B) of H2KO and WT mice after the 7-day cold exposure, n=5-7/group in (A) and n=3/group in (B). *p<0.05 by unpaired two-tailed Student's t-test.

(C)-(D) Immunoblotting of mitochondrial respiratory chain complex proteins in iBAT (C) and iWAT (D) of AH2Tg and WT mice after the 7-day cold exposure, n=3/group. *p<0.05 by unpaired two-tailed Student's t-test.

All data are expressed as mean ± SEM.

Figure 7. SUV420H2 regulates brown/beige adipocyte thermogenesis through post-transcriptional regulation of PGC1α protein levels.

(A)-(B) PGC1α mRNA (A) and Protein (B) levels in iWAT of C57B6/6J mice during postnatal development, n=5/group in (A) and n=3/group in (B). *p<0.05 by unpaired two-tailed Student's t-test.

(C)-(D) PGC1α mRNA (C) and Protein (D) levels in iWAT of C57B6/6J mice during cold exposure, n=4/group. In (C), bars with a different letter indicate statistical significance at p<0.05 as analyzed by one-way ANOVA followed by Tukey's multiple comparisons test; in (D), *p<0.05 by unpaired two-tailed Student's t-test.

(E)-(F) PGC1α protein levels in iBAT (E) and iWAT (F) of H2KO and WT mice after the 7-day cold exposure, n=6/group. *p<0.05 by unpaired two-tailed Student's t-test.

(G)-(H) PGC1α protein levels in iBAT (G) and iWAT (H) of AH2Tg and WT mice after the 7-day cold exposure, n=3/group. *p<0.05 by unpaired two-tailed Student's t-test.

All data are expressed as mean ± SEM.

Figure 8. 4E-BP1 mRNA and protein levels are reciprocally regulated in H2KO and AH2Tg animals after cold exposure.

(A) ATAC-seq analysis of chromatin accessibility and RNAseq peak data at *4e-bp1* gene locus in AH2Tg and WT mice after a 7-day cold exposure.

(B)-(C) Expression of *4e-bp1* in various adipose tissues of H2KO (B) and AH2Tg (C) mice after cold exposure, n=5/group in (B), and n=7 (WT) and 6 (AH2Tg in (C). *p<0.05 by unpaired two-tailed Student's t-test.

(D)-(E) 4E-BP1 protein levels in iBAT (D) and iWAT (E) of H2KO and WT mice after the 7-day cold exposure, n=7 (WT) and 5 (H2KO). *p<0.05 by unpaired two-tailed Student's t-test. Blots were run in parallel at the same time.

(F)-(G) 4E-BP1 protein levels in iBAT (F) and iWAT (G) of AH2Tg and WT mice after the 7-day cold exposure, n=8 (WT) and 7 (AH2Tg) in (F), and n=6 (WT) and 9 (AH2Tg) in (G). *p<0.05 by unpaired two-tailed Student's t-test.

(H) 4E-BP1 protein levels in iWAT of C57BL/6J mice during postnatal development and after a cold challenge, n=3/group. Bars with a different letter indicate statistical significance at p<0.05 as analyzed by one-way ANOVA followed by Tukey's multiple comparisons test. Blots were run in parallel at the same time.

All data are expressed as mean ± SEM.

Figure 9. SUV420H2 regulates PGC1α protein levels through increasing H4K20me3 at *4e-bp1* promoter.

(A)-(B) H4K20me3 levels at the promoter regions of *4e-bp1* as assessed by ChIP assay in iBAT (A) and iWAT (B) of H2KO and WT mice after a 7-day cold exposure, n=3/group. *p<0.05 by two-way ANOVA followed by Tukey's multiple comparisons test.

(C)-(D) H4K20me3 levels at the promoter regions of *4e-bp1* as assessed by ChIP assay in iBAT (C) and iWAT (D) of AH2Tg and WT mice after a 7-day cold exposure, n=3/group. *p<0.05 by two-way ANOVA followed by Tukey's multiple comparisons test.

(E)-(F) Basal and NE-induced 4E-BP1 (E), and PGC1α (F) protein levels in BAT1 brown adipocytes treated with either *Suv420h2* knockdown or combined *Suv420h2/4e-bp1* knockdown, n=4-6/group. In (E), Bars with a different letter indicate statistical significance at $p<0.05$ as analyzed by two-way ANOVA followed by Tukey's multiple comparisons test. In (F), *$p<0.05$ by two-way ANOVA followed by Tukey's multiple comparisons test.

All data are expressed as mean ± SEM.

Figure 10. SUV420H2 regulates diet-induced obesity.

(A)-(D) Body weight (A), fat pad mass (B), glucose tolerance test (GTT) (C) and insulin tolerance test (ITT) (D) in H2KO and WT mice fed a HFD when housed at thermoneutralty,. In (A) and (B), n=7/group. *$p<0.05$ by two-way ANOVA with repeated measures followed by Tukey's multiple comparisons test in (A) and unpaired two-tailed Student's t-test in (B). In (C) and (D), n=6-7/group. *$p<0.05$ by two-way ANOVA with repeated measures followed by Tukey's multiple comparisons test.

(E)-(H) Body weight (E), fat pad mass (F), glucose tolerance test (GTT) (G) and insulin tolerance test (ITT) (H) in AH2Tg and WT mice fed a HFD when housed at thermoneutralty. n=6-7/group. *$p<0.05$ by two-way ANOVA with repeated measures followed by Tukey's multiple comparisons test in (E), (G) and (H), and unpaired two-tailed Student's t-test in (F). In (G) and (H), n=6-7/group. *$p<0.05$ by two-way ANOVA with repeated measures followed by Tukey's multiple comparisons test.

All data are expressed as mean ± SEM.

Figure 1

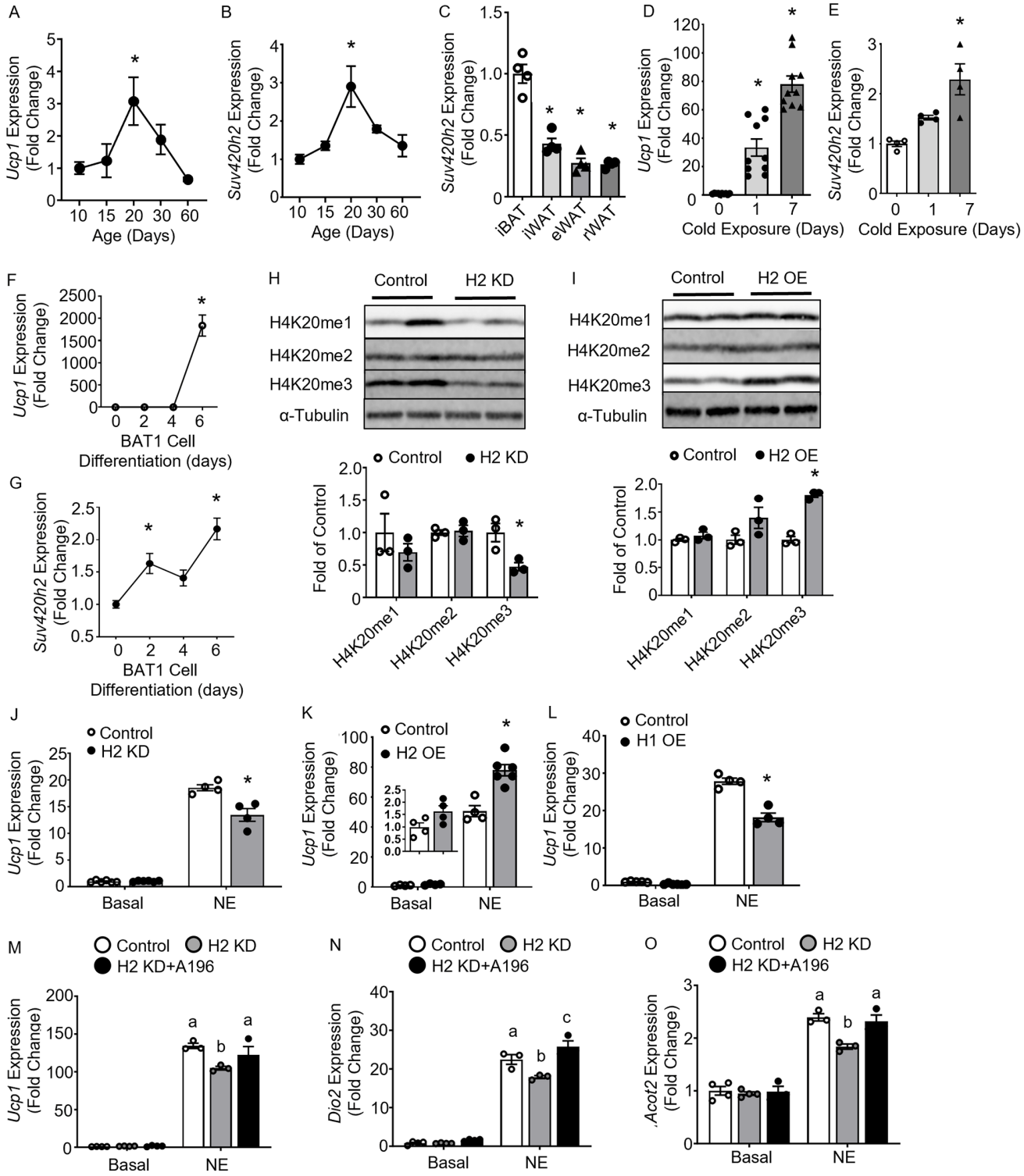
A
Ucp1 Expression (Fold Change)
Age (Days)
B
Suv420h2 Expression (Fold Change)
Age (Days)
C
Suv420h2 Expression (Fold Change)
iBAT
iWAT
eWAT
rWAT
D
Ucp1 Expression (Fold Change)
Cold Exposure (Days)
E
Suv420h2 Expression (Fold Change)
Cold Exposure (Days)
F
Ucp1 Expression (Fold Change)
BAT1 Cell Differentiation (days)
G
Suv420h2 Expression (Fold Change)
BAT1 Cell Differentiation (days)
H
Control
H2 KD
H4K20me1
H4K20me2
H4K20me3
α-Tubulin
Fold of Control
I
Control
H2 OE
H4K20me1
H4K20me2
H4K20me3
α-Tubulin
Fold of Control
J
Control
H2 KD
Ucp1 Expression (Fold Change)
Basal
NE
K
Control
H2 OE
Ucp1 Expression (Fold Change)
Basal
NE
L
Control
H1 OE
Ucp1 Expression (Fold Change)
Basal
NE
M
Control
H2 KD
H2 KD+A196
Ucp1 Expression (Fold Change)
Basal
NE
N
Control
H2 KD
H2 KD+A196
Dio2 Expression (Fold Change)
Basal
NE
O
Control
H2 KD
H2 KD+A196
Acot2 Expression (Fold Change)
Basal
NE

Figure 2

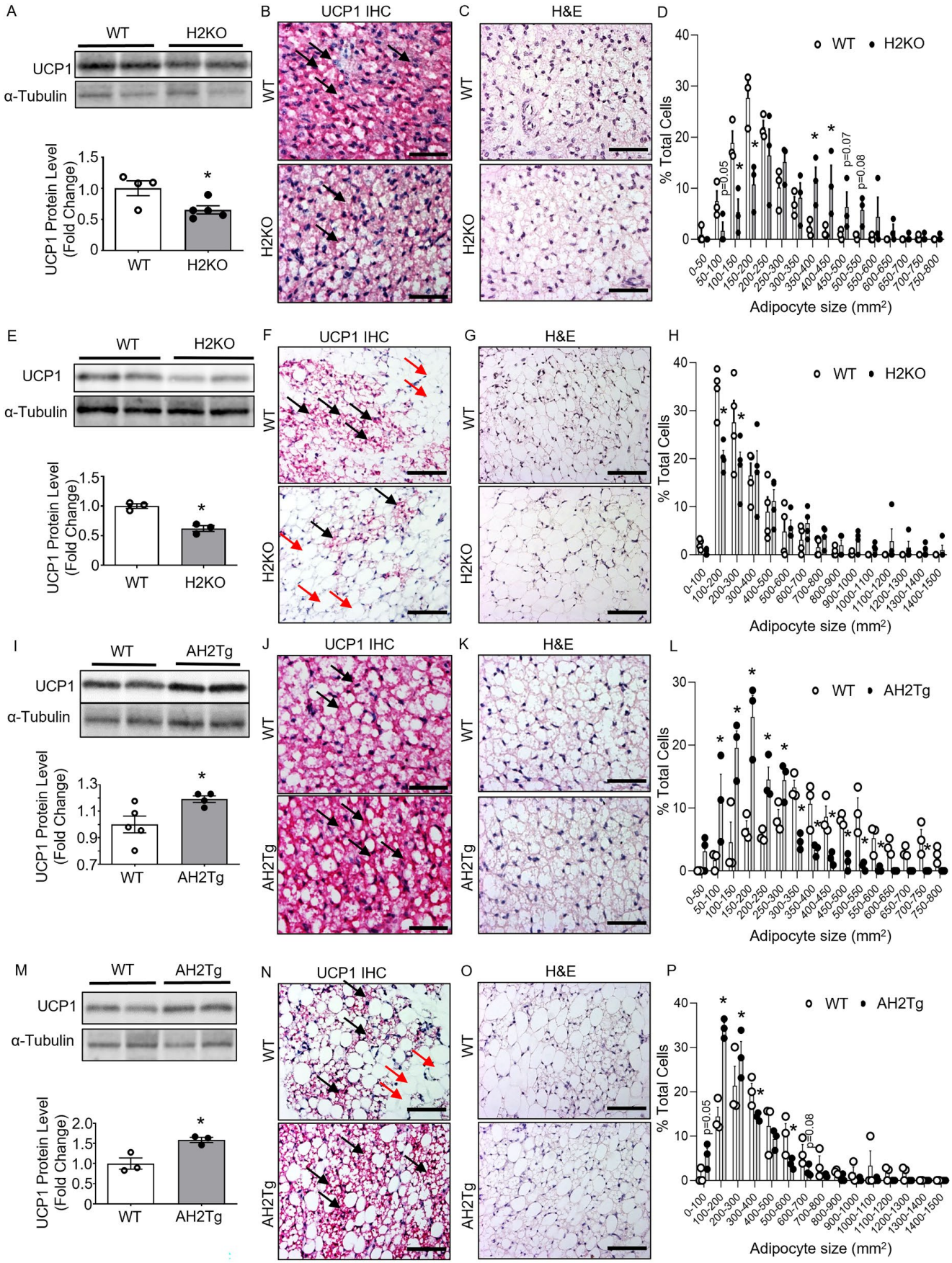
A
WT
H2KO
UCP1
α-Tubulin
UCP1 Protein Level (Fold Change)
B
UCP1 IHC
C
H&E
D
% Total Cells
Adipocyte size (mm²)
p=0.05
p=0.07
p=0.08
E
F
G
H
I
AH2Tg
J
K
L
M
N
O
P

Figure 3

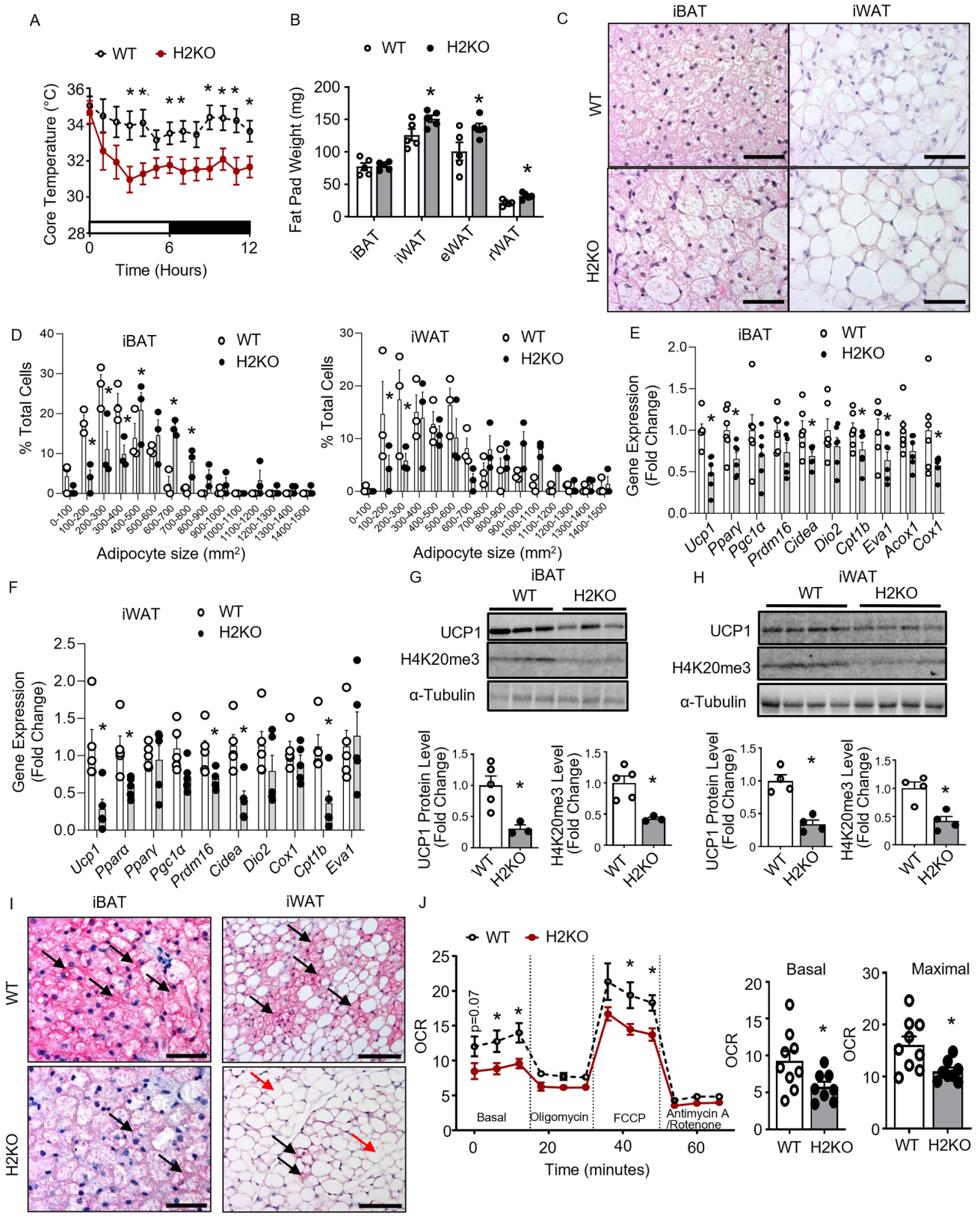
A
WT
H2KO
Core Temperature (°C)
Time (Hours)
B
Fat Pad Weight (mg)
iBAT
iWAT
eWAT
rWAT
C
iBAT
iWAT
WT
H2KO
D
iBAT
iWAT
% Total Cells
Adipocyte size (mm²)
E
Gene Expression (Fold Change)
Ucp1
Pparγ
Pgc1α
Prdm16
Cidea
Dio2
Cpt1b
Eva1
Acox1
Cox1
F
Pparα
G
UCP1
H4K20me3
α-Tubulin
UCP1 Protein Level (Fold Change)
H4K20me3 Level (Fold Change)
H
I
J
OCR
p=0.07
Basal
Oligomycin
FCCP
Antimycin A /Rotenone
Time (minutes)
Maximal

Figure 4

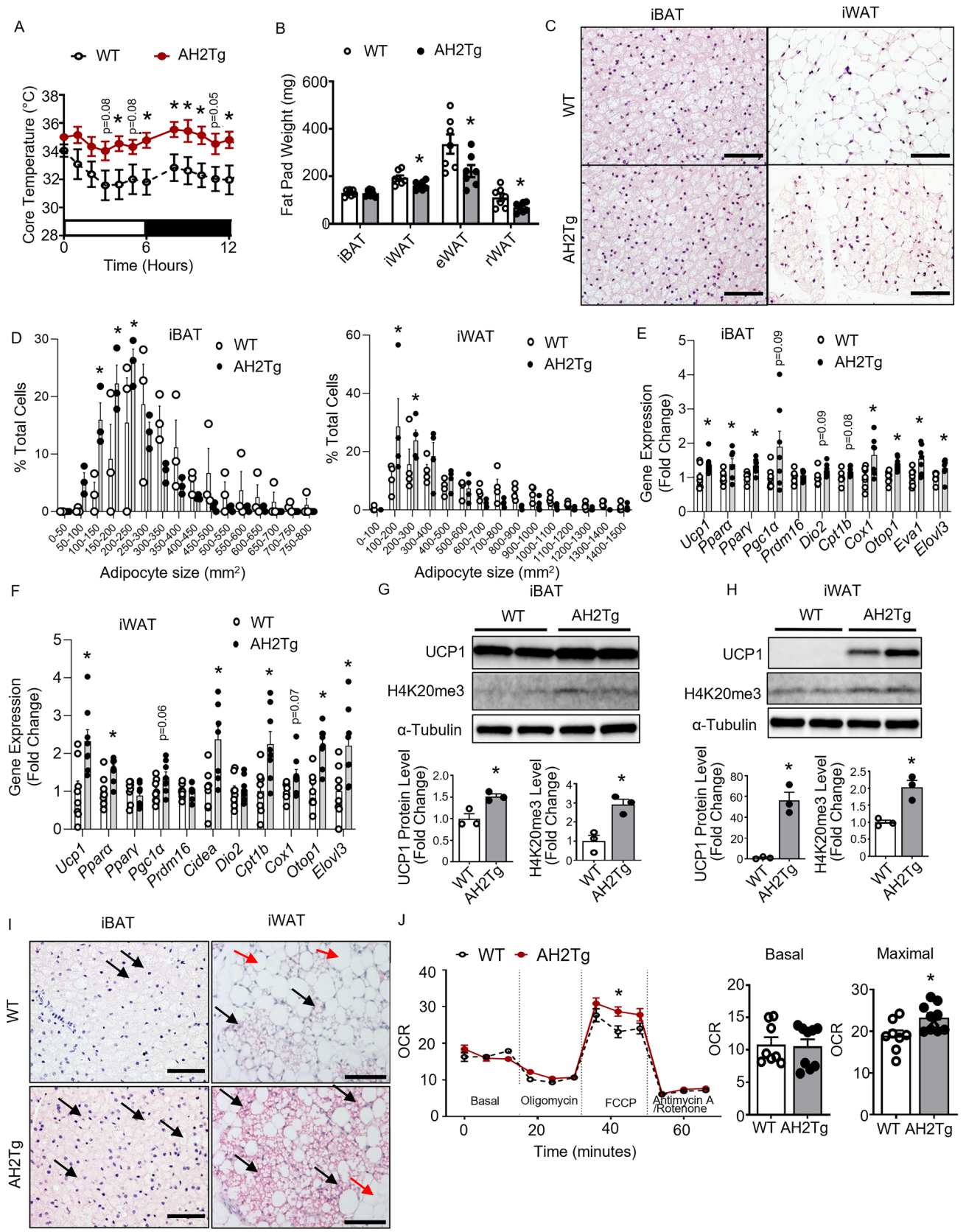
A
WT
AH2Tg
Core Temperature (°C)
Time (Hours)
p=0.08
p=0.08
p=0.05
B
WT
AH2Tg
Fat Pad Weight (mg)
iBAT
iWAT
eWAT
rWAT
C
iBAT
iWAT
WT
AH2Tg
D
iBAT
iWAT
WT
AH2Tg
% Total Cells
Adipocyte size (mm²)
E
iBAT
WT
AH2Tg
Gene Expression (Fold Change)
p=0.09
p=0.09
p=0.08
Ucp1
Pparα
Pparγ
Pgc1α
Prdm16
Dio2
Cpt1b
Cox1
Otop1
Eva1
Elovl3
F
iWAT
WT
AH2Tg
Gene Expression (Fold Change)
p=0.06
p=0.07
Ucp1
Pparα
Pparγ
Pgc1α
Prdm16
Cidea
Dio2
Cpt1b
Cox1
Otop1
Elovl3
G
iBAT
WT
AH2Tg
UCP1
H4K20me3
α-Tubulin
UCP1 Protein Level (Fold Change)
H4K20me3 Level (Fold Change)
H
iWAT
WT
AH2Tg
UCP1
H4K20me3
α-Tubulin
UCP1 Protein Level (Fold Change)
H4K20me3 Level (Fold Change)
I
iBAT
iWAT
WT
AH2Tg
J
WT
AH2Tg
OCR
Basal
Oligomycin
FCCP
Antimycin A /Rotenone
Time (minutes)
Basal
Maximal
OCR
WT
AH2Tg

Figure 5

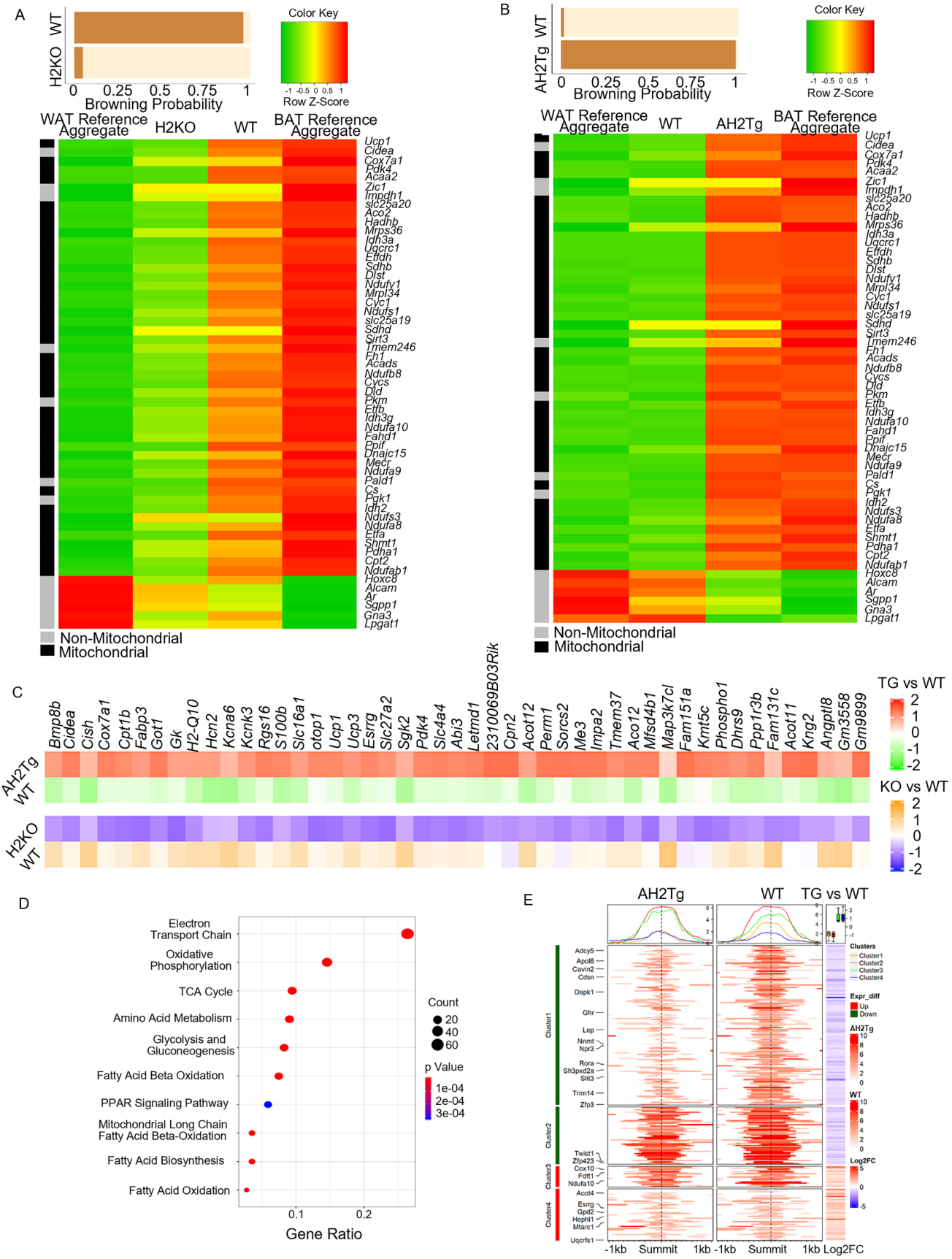
A
WT
H2KO
0 0.25 0.5 0.75 1
Browning Probability
Color Key
-1 -0.5 0 0.5 1
Row Z-Score
WAT Reference Aggregate
H2KO
WT
BAT Reference Aggregate
Ucp1
Cidea
Cox7a1
Pdk4
Acaa2
Zic1
Impdh1
slc25a20
Aco2
Hadhb
Mrps36
Idh3a
Ugcrc1
Etfdh
Sdhb
Dlst
Ndufv1
Mrpl34
Cyc1
Ndufs1
slc25a19
Sdhd
Sirt3
Tmem246
Fh1
Acads
Ndufb8
Cycs
Dld
Pkm
Etfb
Idh3g
Ndufa10
Fahd1
Ppif
Dnajc15
Mecr
Ndufa9
Pald1
Cs
Pgk1
Idh2
Ndufs3
Ndufa8
Etfa
Shmt1
Pdha1
Cpt2
Ndufab1
Hoxc8
Alcam
Ar
Sgpp1
Gna3
Lpgat1
Non-Mitochondrial
Mitochondrial
B
AH2Tg
WT
0 0.25 0.5 0.75 1
Browning Probability
Color Key
-1 -0.5 0 0.5 1
Row Z-Score
WAT Reference Aggregate
WT
AH2Tg
BAT Reference Aggregate
Non-Mitochondrial
Mitochondrial
C
Bmp8b
Cidea
Cish
Cox7a1
Cpt1b
Fabp3
Got1
Gk
H2-Q10
Hcn2
Kcna6
Kcnk3
Rgs16
S100b
Slc16a1
otop1
Ucp1
Ucp3
Esrrg
Slc27a2
Sgk2
Pdk4
Slc4a4
Abi3
Letmd1
2310069B03Rik
Cpn2
Acot12
Perm1
Sorcs2
Me3
Impa2
Tmem37
Aco12
Mfsd4b1
Map3k7cl
Fam151a
Kmt5c
Phospho1
Dhrs9
Ppp1r3b
Fam131c
Acot11
Kng2
Angptl8
Gm3558
Gm9899
AH2Tg
WT
H2KO
WT
TG vs WT
2
1
0
-1
-2
KO vs WT
2
1
0
-1
-2
D
Electron Transport Chain
Oxidative Phosphorylation
TCA Cycle
Amino Acid Metabolism
Glycolysis and Gluconeogenesis
Fatty Acid Beta Oxidation
PPAR Signaling Pathway
Mitochondrial Long Chain Fatty Acid Beta-Oxidation
Fatty Acid Biosynthesis
Fatty Acid Oxidation
0.1
0.2
Gene Ratio
Count
20
40
60
p Value
1e-04
2e-04
3e-04
E
AH2Tg
WT
TG vs WT
Cluster1
Cluster2
Cluster3
Cluster4
Adcy5
Apol6
Cavin2
Cdsn
Dapk1
Ghr
Lep
Nnmt
Npr3
Rora
Sh3pxd2a
Slit3
Trim14
Zfp3
Twist1
Zfp423
Cox10
Fdft1
Ndufa10
Acot4
Esrrg
Gpd2
Hephl1
Mtarc1
Uqcrfs1
Clusters
Cluster1
Cluster2
Cluster3
Cluster4
Expr_diff
Up
Down
AH2Tg
WT
Log2FC
-1kb
Summit
1kb
-1kb
Summit
1kb
Log2FC

Figure 6

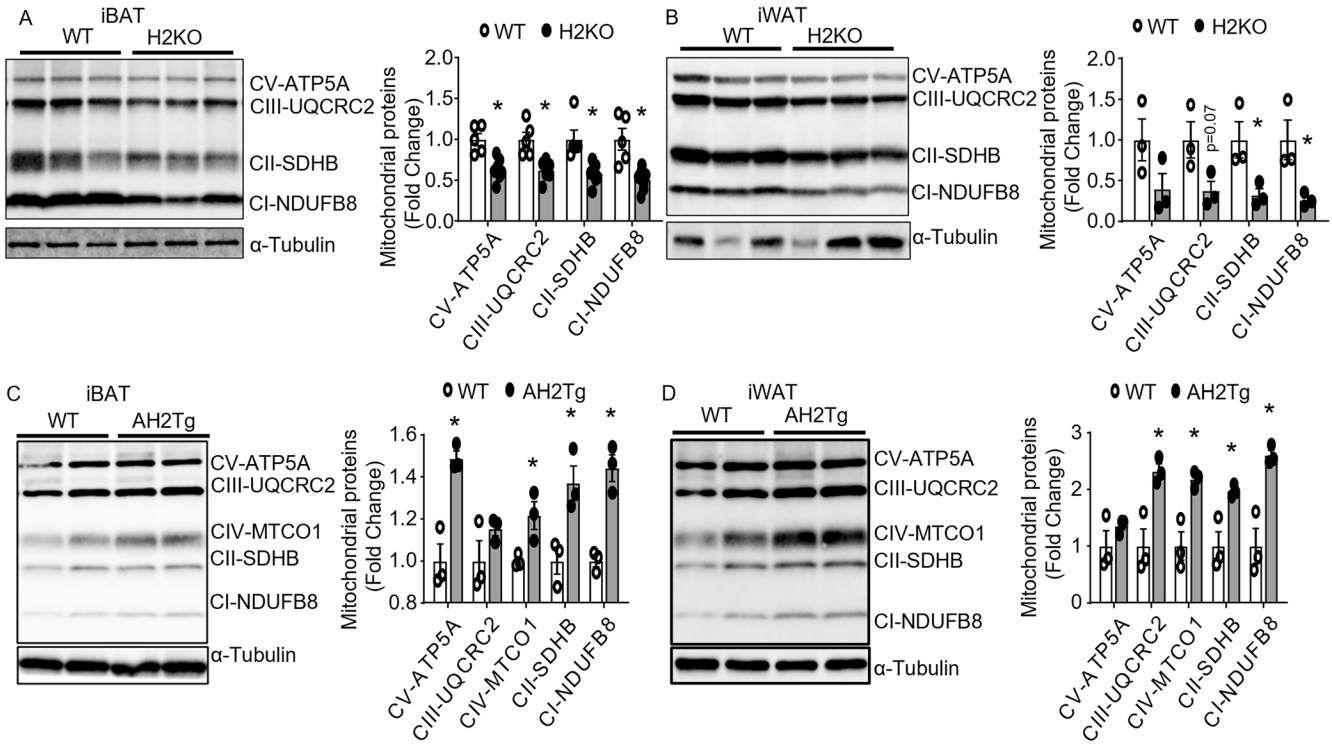
A
iBAT
WT
H2KO
CV-ATP5A
CIII-UQCRC2
CII-SDHB
CI-NDUFB8
α-Tubulin
WT
H2KO
Mitochondrial proteins (Fold Change)
CV-ATP5A
CIII-UQCRC2
CII-SDHB
CI-NDUFB8
B
iWAT
WT
H2KO
CV-ATP5A
CIII-UQCRC2
CII-SDHB
CI-NDUFB8
α-Tubulin
WT
H2KO
p=0.07
Mitochondrial proteins (Fold Change)
CV-ATP5A
CIII-UQCRC2
CII-SDHB
CI-NDUFB8
C
iBAT
WT
AH2Tg
CV-ATP5A
CIII-UQCRC2
CIV-MTCO1
CII-SDHB
CI-NDUFB8
α-Tubulin
WT
AH2Tg
Mitochondrial proteins (Fold Change)
CV-ATP5A
CIII-UQCRC2
CIV-MTCO1
CII-SDHB
CI-NDUFB8
D
iWAT
WT
AH2Tg
CV-ATP5A
CIII-UQCRC2
CIV-MTCO1
CII-SDHB
CI-NDUFB8
α-Tubulin
WT
AH2Tg
Mitochondrial proteins (Fold Change)
CV-ATP5A
CIII-UQCRC2
CIV-MTCO1
CII-SDHB
CI-NDUFB8

Figure 7

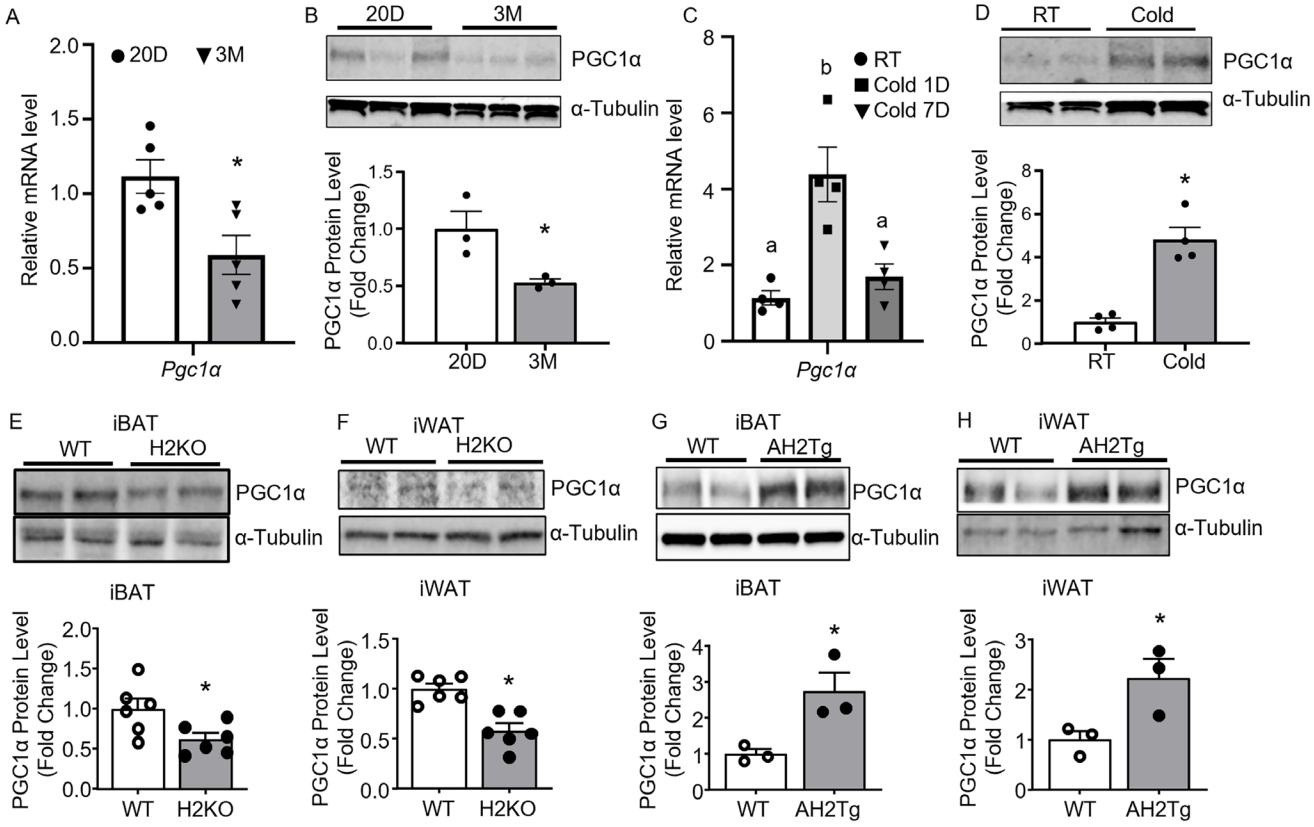
A
20D
3M
Relative mRNA level
Pgc1α
B
20D
3M
PGC1α
α-Tubulin
PGC1α Protein Level (Fold Change)
C
RT
Cold 1D
Cold 7D
Relative mRNA level
Pgc1α
D
RT
Cold
PGC1α
α-Tubulin
PGC1α Protein Level (Fold Change)
E
iBAT
WT
H2KO
PGC1α
α-Tubulin
F
iWAT
WT
H2KO
PGC1α
α-Tubulin
G
iBAT
WT
AH2Tg
PGC1α
α-Tubulin
H
iWAT
WT
AH2Tg
PGC1α
α-Tubulin

Figure 8

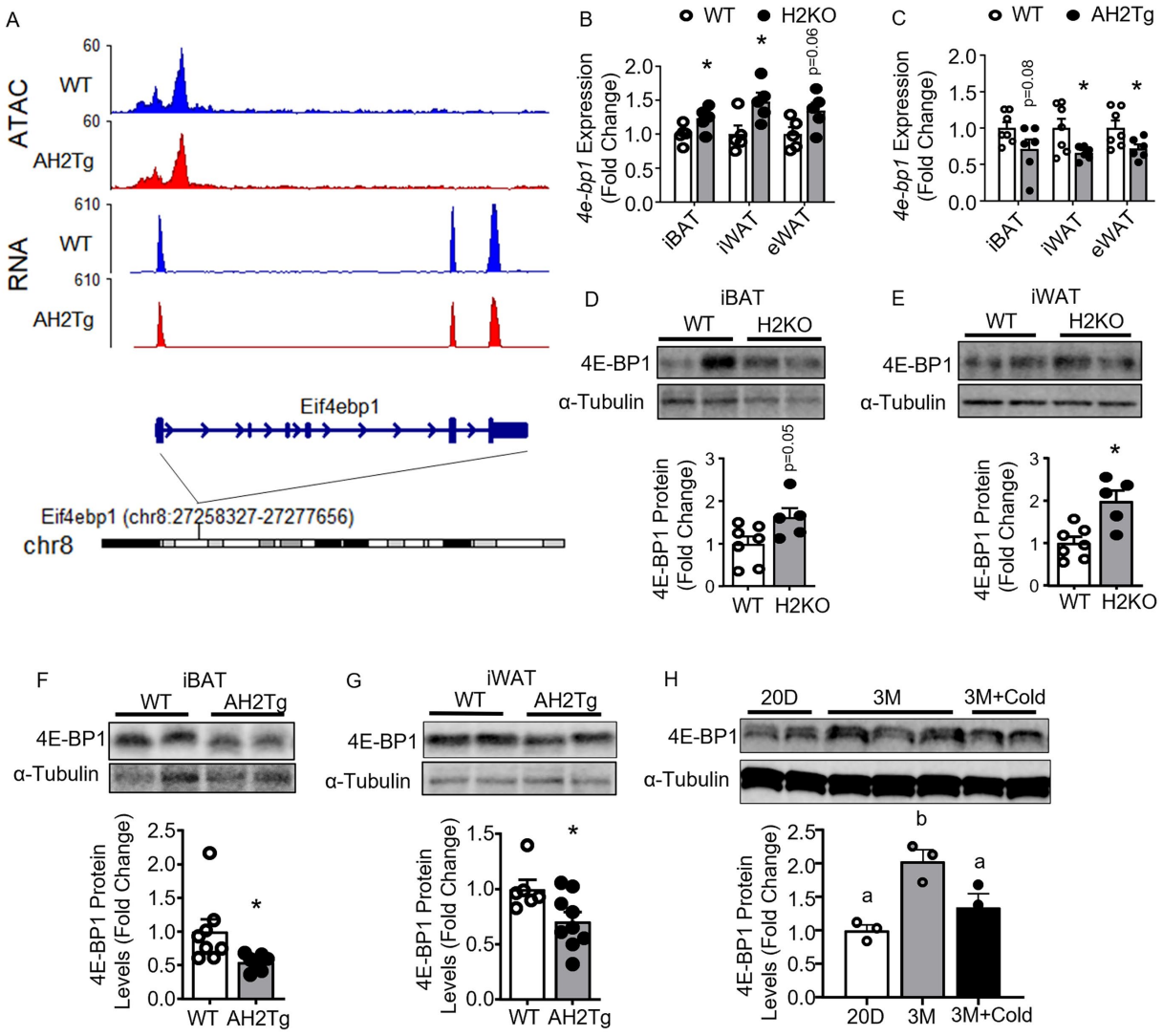
A
ATAC
WT
AH2Tg
RNA
WT
AH2Tg
Eif4ebp1
Eif4ebp1 (chr8:27258327-27277656)
chr8
B
WT
H2KO
4e-bp1 Expression (Fold Change)
iBAT
iWAT
eWAT
p=0.06
C
WT
AH2Tg
4e-bp1 Expression (Fold Change)
p=0.08
D
iBAT
WT
H2KO
4E-BP1
α-Tubulin
4E-BP1 Protein (Fold Change)
p=0.05
E
iWAT
F
iBAT
AH2Tg
4E-BP1 Protein Levels (Fold Change)
G
iWAT
H
20D
3M
3M+Cold

Figure 9

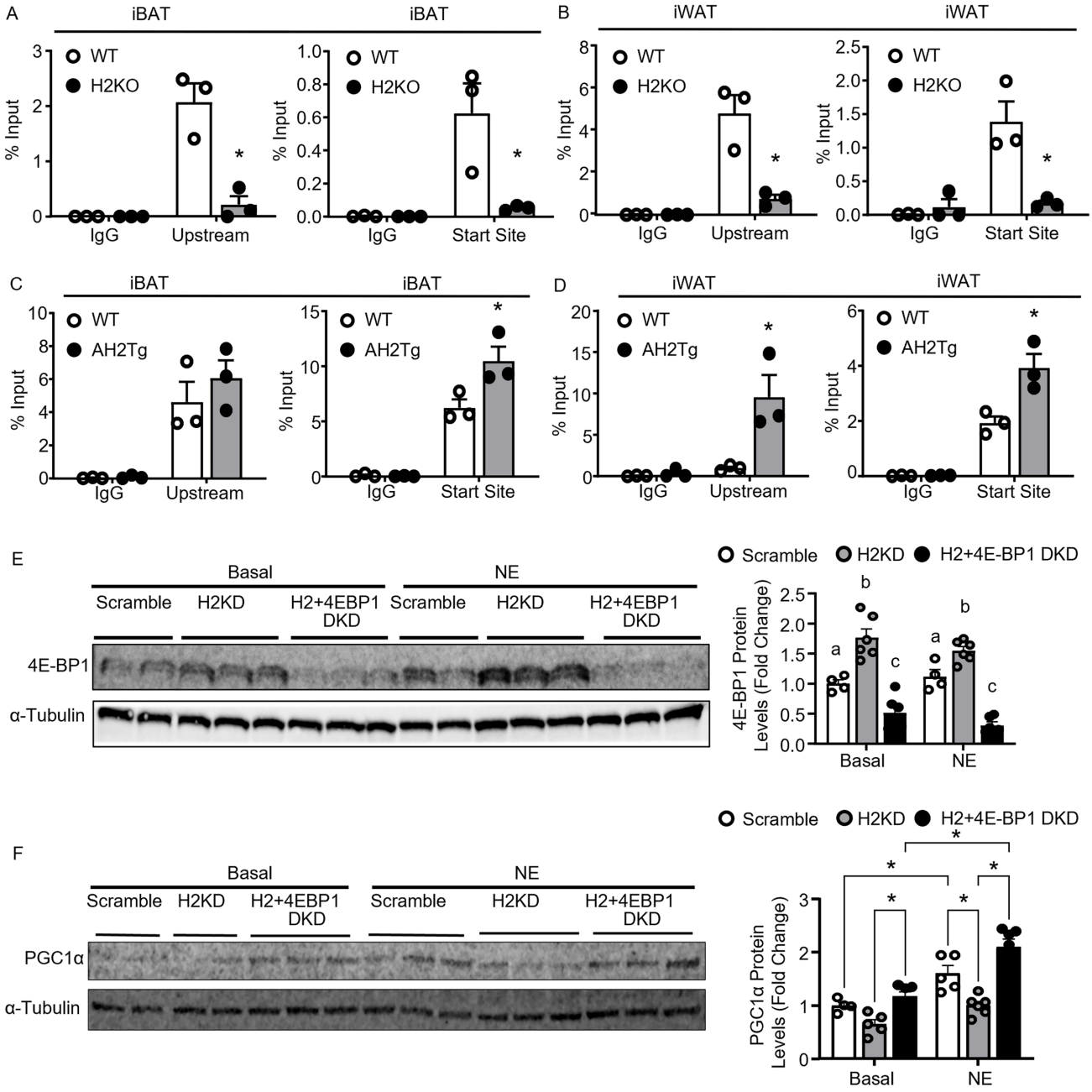
A
iBAT
iBAT
WT
H2KO
% Input
IgG
Upstream
Start Site
B
iWAT
iWAT
C
AH2Tg
D
E
Basal
NE
Scramble
H2KD
H2+4EBP1 DKD
4E-BP1
α-Tubulin
Scramble H2KD H2+4E-BP1 DKD
4E-BP1 Protein Levels (Fold Change)
F
PGC1α
PGC1α Protein Levels (Fold Change)

Figure 10

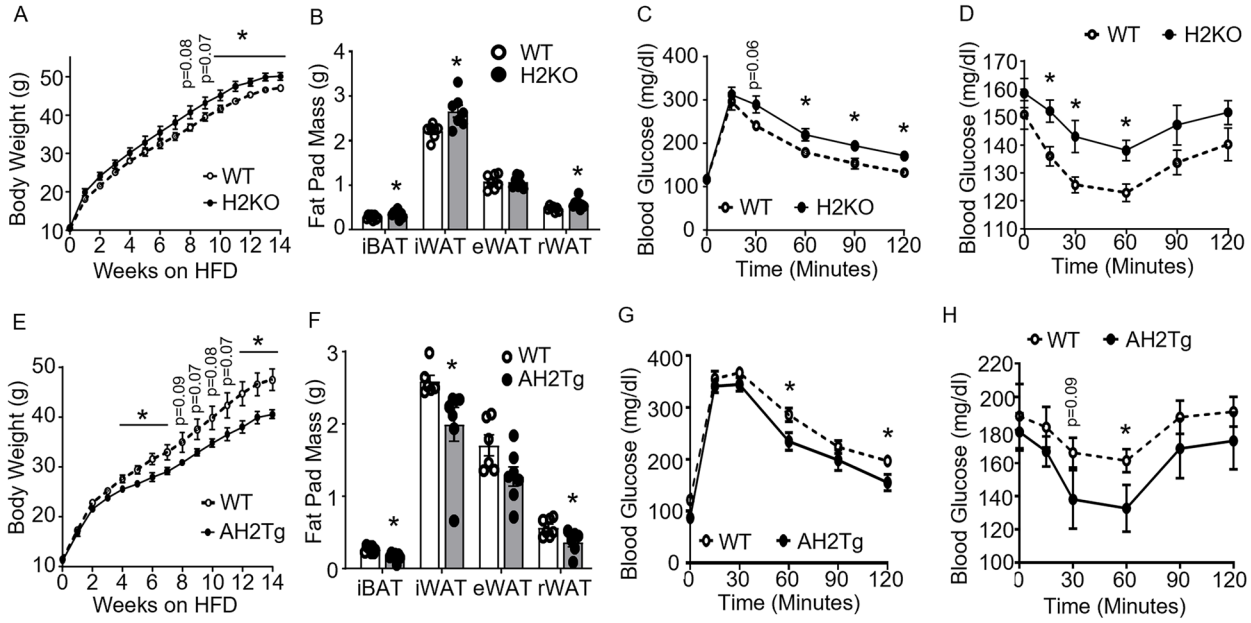
A
Body Weight (g)
Weeks on HFD
WT
H2KO
p=0.08
p=0.07
B
Fat Pad Mass (g)
iBAT iWAT eWAT rWAT
C
Blood Glucose (mg/dl)
Time (Minutes)
p=0.06
D
E
F
AH2Tg
p=0.09
G
H